ADVANCING EARTH AND SPACE SCIENCE

Tectonics

RESEARCH ARTICLE

10.1029/2022TC007550

Key Points:

- River longitudinal profiles and low-relief upland surfaces indicated an increasing vertical deformation toward the eastern Central Taurides
- Geomorphic markers constrained mean cumulative 1,710 ± 50 m surface uplift that peaks in the quadrangle of Alanya-Başyayla-Ermenek-Gazipaşa
- Kinematic indicators from the youngest brittle structures revealed an active NE-SW extension above the Cyprus Subduction Zone

Correspondence to:

T. Aykut,
aykut20@itu.edu.tr

Citation:

Aykut, T., Yıldırım, C., & Uysal, I. T. (2023). Active deformation pattern in the western flank of the Central Taurides, southern margin of the Central Anatolian Plateau: Inferences from geomorphic markers and kinematic indicators. *Tectonics*, *42*, e2022TC007550. https://doi.org/10.1029/2022TC007550

Received 17 AUG 2022
Accepted 10 MAY 2023

Active Deformation Pattern in the Western Flank of the Central Taurides, Southern Margin of the Central Anatolian Plateau: Inferences From Geomorphic Markers and Kinematic Indicators

Tunahan Aykut[1], Cengiz Yıldırım[1], and I. Tonguç Uysal[2,3]

[1]Eurasia Institute of Earth Sciences, Istanbul Technical University, Istanbul, Turkey, [2]School of Earth and Environmental Sciences, The University of Queensland, Brisbane, QLD, Australia, [3]Department of Geological Engineering, Faculty of Engineering, Istanbul University-Cerrahpasa, Istanbul, Turkey

Abstract The southwestern margin of the Central Anatolian Plateau corresponds to the upper crust of the subduction between African and Anatolian plates, with a high relief of up to 2 km. This mountainous region has distinctive geomorphological features and presents a unique setting to investigate the mechanism of orogenic plateau margin development related to subduction and topographic evolution around the Eastern Mediterranean. We present new kinematic data from exposed fault planes and tectonic landforms from high-resolution digital elevation models to elucidate the deformation pattern and its relation with the crustal deformation. We evaluate the deformation pattern based on the spatial distribution of kinematic analyses and geomorphic markers like low relief upland surfaces, disrupted karst basins, knickpoints, and deep bedrock incisions from watershed to shoreline. Our geomorphic analysis reveals a post-orogenic transient actively deforming topography. The geomorphic markers constrain long-term surface uplift pattern with a mean cumulative surface uplift of 1,710 ± 50 m and shows an increasing trend from west to east, from 1,600 ± 50 to 1,800 ± 50 m. Our results suggest a dome-like uplift pattern in the west-east direction across the southern margin that reaches up to maximum cumulative uplift values in the quadrangle of Alanya-Başyayla-Ermenek-Gazipaşa. Our kinematic measurements along the youngest generation of faults revealed an active NE-SW extensional deformation across a broad 200 km zone in the north of the subduction. Our findings have significant implications for understanding the morphotectonic evolution and post-orogenic deformation in the plateau margins and geodynamic evolution of the Eastern Mediterranean.

1. Introduction

Orogenic plateaus such as Tibetan and Central Andean Plateaus are major topographical features on the Earth's surface, reflecting the complex relationships between mantle, crustal and surface processes (Allmendinger et al., 1997; Cheng et al., 2019; Çiner et al., 2015; Facenna et al., 2014; Husson, 2006; Schildgen et al., 2012a, 2014). Geomorphic and geological records at orogenic plateau margins enable the understanding of the history of horizontal and vertical plate movements (Kirby et al., 2000; Masek et al., 1994; Pingel et al., 2019; Strecker et al., 2009; Vandervoot et al., 1995; Yıldırım et al., 2011, 2013). Central Anatolia in the Eastern Mediterranean exhibits a high elevated-low relief landscape known as the Central Anatolian Plateau (CAP) (Figure 1a). CAP has evolved into a prominent landscape in the junction of the complex geodynamic mechanisms, which was governed by the convergence between African and Eurasian plates and following collision between Anatolian and Arabian Plates in the Early-Middle Miocene (Okay et al., 2010; Şengör & Yılmaz, 1981). This orogenic plateau is located in the transition zone between Western Anatolian Extensional and Eastern Anatolian Contractional Neotectonic Provinces (Şengör et al., 1985) with an average of 1,000 m elevation and bounded by Pontides and Taurides mountain ranges in its northern and southern margins, respectively (Figure 1a). As an orogenic plateau, the CAP and its margins exhibit prominent geological and geomorphological features to better understand the geodynamic evolution of the Eastern Mediterranean region (Cosentino et al., 2012; Facenna and Becker, 2020; Fernández-Blanco et al., 2019, 2020; Howell et al., 2017; Meijers et al., 2018; McPhee et al., 2018; Öğretmen et al., 2018; Radeff et al., 2017; Racano et al., 2021; Schildgen et al., 2012a, 2012b, 2014; Yıldırım et al., 2011, 2013, 2016).

Margins of the CAP have higher topographic relief than the plateau interior, implying the different modes of active deformation. While the active deformation and surface uplift in the northern margin of the CAP has

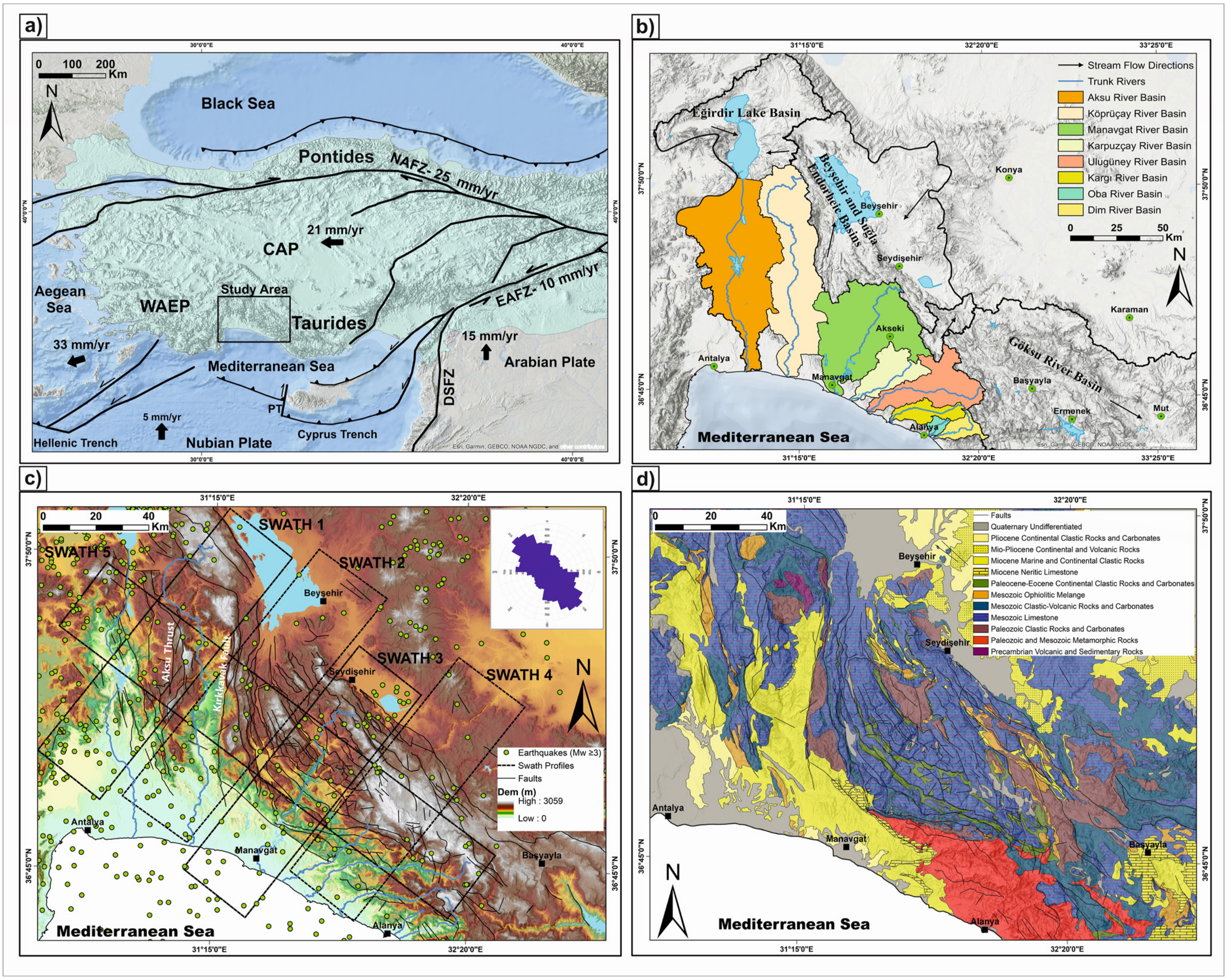

Figure 1. (a) Simplified active tectonic map of the Eastern Mediterranean and Anatolia. The black box indicates the study area. Black arrows denote the movement directions relative to Eurasia. GPS velocities are from Reilinger et al. (2006). CAP: Central Anatolian Plateau; WAEP: West Anatolian Extensional Province; NAFZ: North Anatolian Fault Zone; EAFZ: East Anatolian Fault Zone; DSFZ: Dead Sea Fault Zone; PT: Paphos Transform Fault. (b) The studied drainage basins across the western Central Taurides. (c) The digital elevation model that shows the main topographical features of the study area. Black lines are the main faults and lineaments from the regional geological maps (Şenel, 2002). Black boxes with dashed lines are footprints of topographic swath profiles. Rose diagram of the faults lineament presented as an inlet. Green points represent the earthquakes (Mw 3≤) between 0 and 30 km depths (The data is from "Boğaziçi University-Kandilli Observatory and Earthquake Research Institute," http://www.koeri.boun.edu.tr/sismo/zeqdb/indexeng.asp, and "Disaster and Emergency Management of Turkey (AFAD)," https://deprem.afad.gov.tr/event-catalog.) (d) Simplified lithological map of the study area.

been interpreted as a result of restraining bend and strain accumulation related to the North Anatolian Fault Zone (Yıldırım et al., 2011), numerous studies proposed mantle-related processes like slab tearing, slab break-off and asthenospheric upwelling (Biryol et al., 2011; Cosentino et al., 2012; Facenna et al., 2006; Schildgen et al., 2012a, 2012b, 2014), and lower crustal thermal deformation as a consequence of fore-arc sedimentation (Fernández-Blanco et al., 2020) to explain the surface uplift along the central part of the southern margin of the CAP. In the southern margin of the CAP, the Central Taurides (CT) constitute a 2 km-high relief. This mountainous region has distinctive geological and geomorphological features. It presents a unique setting to investigate mechanisms for orogenic plateau and margin development, subduction-related deformation patterns, and ongoing geodynamics in the Eastern Mediterranean. Most of the previous studies focused on the central and eastern parts of the CT, where horizontal marine sediments crop out at 2,000 m elevation. Using sedimentological, biostratigraphic, and geomorphic evidence, two main surface uplift phases were proposed for the eastern flank of the CT. The first uplift phase commenced at 8 Ma earliest, followed by a second and faster phase starting from 1.6 Ma

(Cosentino et al., 2012; Schildgen et al., 2012a). Radeff et al. (2017) provided a minimum age constraint of 5.45 Ma for the starting time of the first uplift phase. Recently, Öğretmen et al. (2018) proposed an accelerated uplift in the last 450 Kyr as a part of the multi-phased uplift history of the central southern margin. However, this uplift is not uniform, and the whole CT tilts toward the east based on decreasing shoreline elevation angles of older marine terraces (Racano et al., 2020). These studies focused on mainly deep-seated processes with a limited contribution to the upper crustal deformation explaining the landscape evolution. Deep-seated processes can only define the relief, whereas the upper crustal deformation defines the texture (e.g., ruggedness) of topography. The landscape evolution models neglecting this interaction might be inadequate for understanding plateau margin developments, especially in regions with a high fault density.

Schildgen et al. (2012b) proposed a mantle-driven uplift model and stated that the uplift in the western flank started in the late Miocene. However, the questions about the mode and mechanism of the upper crustal deformation and the uplift pattern need to be investigated more. In this context, we focused on the kinematics of faults and their influence on topography, together with regional geomorphic markers such as low-relief relic upland surfaces, river profiles (e.g., knickzones), disrupted karst basins, and deep bedrock incision from drainage divides to the shoreline. We blended kinematic data from exposed fault planes and tectonic geomorphology from high-resolution digital elevation models (DEMs) to provide a deformation model considering deep-seated and upper crustal processes in the western flank.

2. Geological Setting

The western flank contains rocks from the Precambrian to the Quaternary (Akay & Uysal, 1988; Özgül, 1976; Schmid et al., 2020). Basement units consist of the Mesozoic autochthonous carbonate limestones which were deposited in the Neotethys Ocean (Şengör & Yılmaz, 1981; Schmid et. al., 2020). Özgül (1976) named this unit as Geyikdağı Autochthonous Unit. This basement is overthrust by allochthonous Beyşehir-Hoyran, Antalya, and Alanya Nappes which consist of Paleozoic-Mesozoic ophiolitic melanges, metamorphic rocks, limestones, and Eocene carbonates-clastics (Özgül, 1976) (Figure 1d). In the southern part of the study area, the Miocene Antalya Basin (Aksu, Manavgat, and Köprüçay Sedimentary Basins) units unconformably overlie the basement units of Geyikdağı Platform Carbonates, Alanya, and Antalya nappes. In the general context, the Antalya Miocene basin consists of Miocene marine to non-marine clastic sediments, Miocene neritic limestones and Pliocene to Recent marine sediments, clastic terrestrials, and travertines. Neogene marine sediments of the Antalya Basin lie at elevations up to 1,500 m today (Çiner et al., 2008; Kanbur & Öğretmen, 2022; Karabıyıkoğlu et al., 2000) (Figure 1d).

A high and steep topography superimposes these geological units. The maximum elevations tend to increase from the western to the eastern parts of the flank, from 2,400–2,500 to 2,800–2,900 m (Figure 1c). There are well-preserved paleo-valleys that perched on a wide paleosurface at elevations of about 2,000 m (Monod et al., 2006). The common presence of limestone is represented by the karst landscape with widespread karst landforms such as tectono-karst poljes, fluvial-karst depressions, ponors, and dolines (Doğan et al., 2017). The general trend of the tectono-karst poljes is comparable with the NW-SE trend of the flank. These relic landscapes and poljes are transversely dissected by eight major river basins from west to east: Aksu, Köprüçay, Manavgat, Karpuzçay, Ulugüney, Kargı, Oba, and Dim. The river network generally flows from north-northeast to south-southwest, toward the Mediterranean Sea (Figure 1b).

The study area has been affected by different stress regimes throughout Neogene and Quaternary times (Glover and Robertson, 1998a, 1998b; Poisson et al., 2003, 2011; Üner et al., 2015). The southwest movement and emplacement of Lycian Nappes onto the Western Taurides has caused the first contractional deformation lasting until the Middle Miocene in the westernmost part of CT (Akay & Uysal, 1988; Flecker et al., 1998). Recently, a NW-SE extensional period was defined by Üner et al. (2015), lasting from Middle to Late Miocene. The westward escape and counterclockwise rotation of the Anatolian microplate triggered a compressional "Aksu Phase" and deformed the Late Miocene-Late Pliocene formations, forming the N-NW trending 100 km long Aksu Thrust Zone (Çiner et al., 2008; Glover & Robertson, 1998b; Poisson et al., 2003, 2011). The last deformational phase is the NE-SW, and E-W directed neotectonic extensional regime that occurred between the latest Pliocene and Recent (Glover & Robertson, 1998b; Howell et al., 2017; Kanbur & Öğretmen, 2022; Schildgen et al., 2012b; Üner et al., 2015).

The Kırkkavak Fault is another major fault that bounds the Köprüçay and Manavgat basins (Figure 1c). The Kırkkavak Fault caused the asymmetric subsidence of the Köprüçay Sedimentary Basin in the Middle Miocene with the normal faulting (Çiner et al., 2008). In the Tortonian, some parts of the Kırkkavak Fault exhibited inversion to a reverse fault as a consequence of the Aksu Phase (Çiner et al., 2008; Karabıyıkoğlu et al., 2000). After this compressional phase, the faulting mechanism evolved into a strike-slip and then to normal faulting in the Quaternary (Glover & Robertson, 1998b; Schildgen et al., 2012b).

Farther east between Seydişehir-Manavgat, the active tectonic deformation history is poorly known. The direction of main lineaments is generally NW-SE and N-S (Figure 1c). Some of these lineaments coincide with the paleotectonic overthrust zones which have formed as a result of the Africa-Eurasia plate convergence (Akay & Uysal, 1988; McPhee et al., 2018). These lineaments were interpreted as the reactivated normal faults due to the extensional neotectonic regime (Doğan et al., 2017; Monod et al., 2006). Schildgen et al. (2012b) argued that these normal faults are formed after the thermally driven uplift of the upper crust as a consequence of asthenospheric upwelling.

3. Data and Methods

To understand the pattern and the spatial distribution of the active deformation, we combined regional geomorphology, morphometric, and kinematic analysis. We utilized high-resolution DEM including 12.5 m resolution The Advanced Land Observing Satellite PALSAR and 30 m resolution Shuttle Radar Topography Mission for morphometric analysis. Red Relief Image Maps (RRIMs) is generated (Chiba et al., 2008) to identify and map tectonic landforms. We used "The TopoToolbox" (Schwanghart & Scherler, 2014) and "The Topographic Analysis Kit" (Forte & Whipple, 2019) for river longitudinal profile and steepness analysis, swath profile, and knickpoint extraction. The "Spatial Analysis" and "3D Analysis" tools of ESRI's ArcGIS 10.7 software were implemented for topographical relief, hydrology, and RRIM analysis. We also used 1/500,000 scale geological maps published by the General Directorate of Mineral Research and Exploration of Turkey (MTA) in 2002.

3.1. Topographical Swath Profiles

Topographical swath profiles can be used to infer the general character of topography throughout the desired area. They show the distribution of maximum, mean and minimum elevations across a given rectangular zone. While the minimum elevations denote the valley floors, maximum elevations correspond to the peaks and ridges, hence they display the variation of the topographical relief along with the given stripes. We extracted five swath profiles. Four of the swath profiles are 30 km wide, 100–120 km long and orthogonal to the CT. One of the swath profiles is 30 km wide and 180 km long, parallel to the regional psychographic trend.

3.2. River Longitudinal Profiles, Channel Steepness, and Knickpoints

The general shape of the river profiles provides information about the interaction between the tectonic and surface processes. Rivers tend to reach a concave-up graded profile in steady tectonic and climatic conditions. Irregularities in the graded profiles and the formation of knickpoints denote deviations from the equilibrium conditions (Demoulin et al., 2012, 2017; Gallen & Wegmann, 2017; Keller & Pinter, 2002; Kirby & Whipple, 2001, 2012; Lague, 2014; Tucker & Whipple, 2002; Wobus et al., 2006). Changing of the equilibrium conditions and formation of knickpoints may result as a consequence of climate changes, fluctuations in sediment load, rock uplift, transient profile evolution, lithological variations and displacements related to active tectonic structures (Gallen, 2018; Hack, 1957; Howard et al., 1994; Kirby et al., 2003; Larue, 2008, 2011).

The steepness index (also referred as normalized steepness index) is the slope of a channel that is normalized to its drainage contribution area. The steepness index (ksn) provides a strong tool for comparing slopes of river channel segments, detecting the deviations in graded river longitudinal profiles and determining deformation patterns (Kirby et al., 2003; Perron & Royden, 2013; Wang et al., 2019; Yıldırım & Tüysüz, 2017). Stream gradient decreases downstream as a power-law function of contributing drainage area (Flint, 1974; Hack, 1973; Wang et al., 2019). This relationship can be expressed as:

$$S = k_s A^{-\theta} \quad (1)$$

where S = channel gradient, A = upstream drainage area, k_s = channel steepness index, and θ = channel concavity index.

Empirical data from different parts and environments around the world showed that the steepness index correlates with lithology, rock uplift and climate (Cyr et al., 2010; Jiang et al., 2016; Kirby et al., 2003; Schildgen et al., 2012a; Snyder et al., 2000; VanLaningham et al., 2006; Whipple, 2004; Wobus et al., 2006). Evaluating steepness index data has been proved successful in detecting tectonic forcing and interpreting its activity (Kirby et al., 2003; Scherler et al., 2014; Whittaker et al., 2008). We used $\theta_{ref} = 0.45$ for steepness index analysis as this value has been accepted and used as the best representative concavity value. This value also varies little across different landscapes and provides a basis for comparing steepness index values across different geomorphological settings (Kirby & Whipple, 2012; Snyder et al., 2000).

In erosional landscapes, identifying knickpoints plays an important role in the interpretation of active tectonic deformation (Keller & Pinter, 2002; Kirby & Whipple, 2012; Pavano et al., 2016). As a response to tectonic perturbations, lithological variations, increasing stream flow rates, increasing sediment flux and landslides; new boundaries forms known as the knickpoints, between the downstream region that is adjusting to the new energy state and the upstream reach where the former state is maintained (Chen et al., 2015; Jaiswara et al., 2019; Kirby & Whipple, 2012). Knickpoints are generally classified as "vertical-step knickpoints" and "slope-break knickpoints," according to the morphology of the channel segments in the slope-area plots. While the formation of vertical-step knickpoints has mostly been related to local heterogeneities in the stream channel (like lithological variations), slope-break knickpoints have been linked to spatiotemporally persistent tectonic forcing (Boulton, 2020; Gailleton et al., 2019; Haviv et al., 2010).

We calculated best-fit steepness index values and analyzed the longitudinal profiles of all trunk bedrock streams in our study area to detect the deviations from the concave-up graded channel profiles. We extracted the knickpoints for the trunk streams using the function "knickpointfinder" of "TopoToolbox" (Schwanghart & Scherler, 2014) utilizing MATLAB software. We prepared slope-area plots of trunk streams in log-log space to investigate the knickpoint morphology. In addition, we carried out inverse distance weighting Interpolation using the calculated ksn values of all orders of stream channels throughout our study area.

3.3. Topographical Relief Analysis and Surface Uplift Estimates

The ruggedness and high relief of topography are footprints of high stream incision and surface uplift in tectonically active areas. Contrarily, low relief topography demonstrates a relatively quiet tectonic state, steady-state equilibrium conditions, and flattened topography by external processes. Therefore, investigating the spatial characterization of the relief across a landscape can provide information about the active deformation pattern (Kirby & Whipple, 2012; Wobus et al., 2006).

Low relief perched upland surfaces are slightly undulated remnants of a pre-existing landscape (Clark et al., 2006; Lv et al., 2020; Stearns, 1967; Whipple et al., 2017). The coexistence of these relic surfaces with the geomorphic units like steep gorges reflects a transient topography that is trying to adjust the changing surface elevation (Clark et al., 2006). Reconstruction of the pre-existing landscape provides a datum for determining the spatial distribution and pattern of the surface uplift. If there are perched relic landscapes where the erosion rates are relatively low, the difference in elevation between the current river at the outlet and the projected relict part of the river at the outlet points out the amount of surface uplift since starting of the deformation (Clark et al., 2006; Kirby & Whipple, 2012; Prince & Spotila, 2013; Schildgen et al., 2012a; Yıldırım & Tüysüz, 2017).

We carried out a local topographic relief analysis for elucidating the pattern of surface uplift. We subtracted minimum elevations from maximum elevations and averaged it over a given 2 km sampling window which demonstrates the valley to ridge relief pattern, and created a local relief map for our study area. We projected paleo-longitudinal profiles for five trunk rivers (Manavgat, Köprüçay, Karpuzçay, Ulugüney, and Dim) where there are relict upland surfaces upstream. We projected the relict channel gradients downstream along their longitudinal profiles, and we estimated the total amount and pattern of the surface uplift along the western flank. In the process of determining paleo-longitudinal channel profiles, we calculated and used best-fit ksn and concavity of channel segments from Equation 1.

3.4. Kinematic Measurements and Paleo-Stress Analysis

To better understand the brittle deformation, we conducted kinematic measurements on fault planes that create topographic lineaments and broad deformation zones between Manavgat-Seydişehir (from coast to plateau). We measured the strike, dip angle, dip direction, and rake features of the fault planes in six key areas (Figure 8). We obtained kinematic data from slickenlines and slicken fibers, which demonstrate the sense of motion between fault blocks.

We used Win-Tensor software (Delvaux & Sperner, 2003) to plot fault-slip data and determine extension and shortening directions. We plotted paleo-stress fields, principal stress directions and related pseudo-fault mechanism solutions. To interpret the spatial distribution of the deformation and identify the changing deformation pattern, we evaluated pseudo-fault mechanism solutions, earthquake focal mechanisms and kinematic data from other studies together (Figure 9a).

4. Results

4.1. Topographical Swath Profiles

Swath profiles orthogonal to the CT (Swath profiles 1–4) denote the controlling effect of the major fault zones over topography. Relief contrasts are widespread in every profile, especially in the transition zones between the mountainous part of the CT and the bounding basins in the northern and southern parts. In the southern part, the topography is relatively smooth, the incision is lower and elevation diminishes toward the Mediterranean Sea. Toward mountainous northern parts, elevations tend to increase, and the topographical scarps are well defined. The boundary between Beyşehir-Suğla depression and CT is controlled by undefined faults, and the transition is very sharp. In each profile, there are major knickzones located at approximately 1,000 and 2,000 m elevations (Figures 2a–2d and 3). These knickzones are mainly controlled by faults. All profiles display recognizable elevated relatively flat surfaces on top of the mountains, between 1,500 and 2,000 m elevation zone.

The swath profile that is parallel to the CT and orthogonal to the main drainage systems (Figure 2e) displays a very rugged morphology across a 180 km zone, with the mountain peaks reaching up to the 3,000 m elevation in the eastern part. Deeply incised valleys are situated in between steep scarps. These scarps are controlled by NW-SE and N-S striking, mostly undefined faults. Swath profile 5 reveals that the elevations tend to increase from west to east along the western flank of the southern margin.

4.2. Longitudinal Profiles, Channel Steepness, and Knickpoints

The longitudinal profiles of the bedrock rivers exhibit deviations from the graded profile. Slope-area plots and ksn values show steepened channel segments, especially in the downstream parts of the major knickzones (Figure 3). Vertical-step knickpoints mainly coincide with the lithological contacts, and some of them are marked by faults and lithological boundaries together. The relatively minor knickpoints are not distinguishable in the slope-area plots because of the scattering of the data across an intensely karstified erosional landscape. Therefore, we further investigated and utilized geological maps and our field observations to classify the knickpoints. We identified the lithological and tectonic knickpoints according to their spatial relation to the lithological and tectonic boundaries. Some of the knickpoints coincide with neither lithological contacts nor tectonic boundaries. These knickpoints are attributed to waves of headward erosion processes. The main slope-break knickzones that coincide with the tectonic lineaments culminate in between 500 and 2,000 m elevations. Relatively minor vertical-step knickpoints are located in the downstream parts of the rivers between 0 and 500 m elevations related to lithological variations and small fault segments. Major slope-break knickzones separate fragments of low relief upland surfaces and steeper channel segments downstream, implying an actively deforming topography. Best-fit ksn values rise up to 713 along the major slope-break knickzones. Both slope-break and vertical-step knickzones are clearly seen in the slope-area plots, as the slopes of the channels display dramatic increases downstream (Figure 4).

In the Aksu Basin, tectonic knickpoints are located upstream of the river, where the trunk stream flows over the segments of the Aksu Thrust Zone (Figure 3a). In the Dim Basin, a very distinct slope-break knickzone is located between 500 and 2,000 m elevations (Figure 3h). The elevation of the trunk stream increases 1,500 m, and the ksn value reaches up to 477 in a very short distance. The distribution of the steepness index values shows an increasing trend from the bounding basins to the higher section of western CT. The ksn values display an increasing trend from the west to east part of the study area, reaching to highest values in the easternmost part of western CT, despite the relatively homogenous lithology (Figures 5a and 5b).

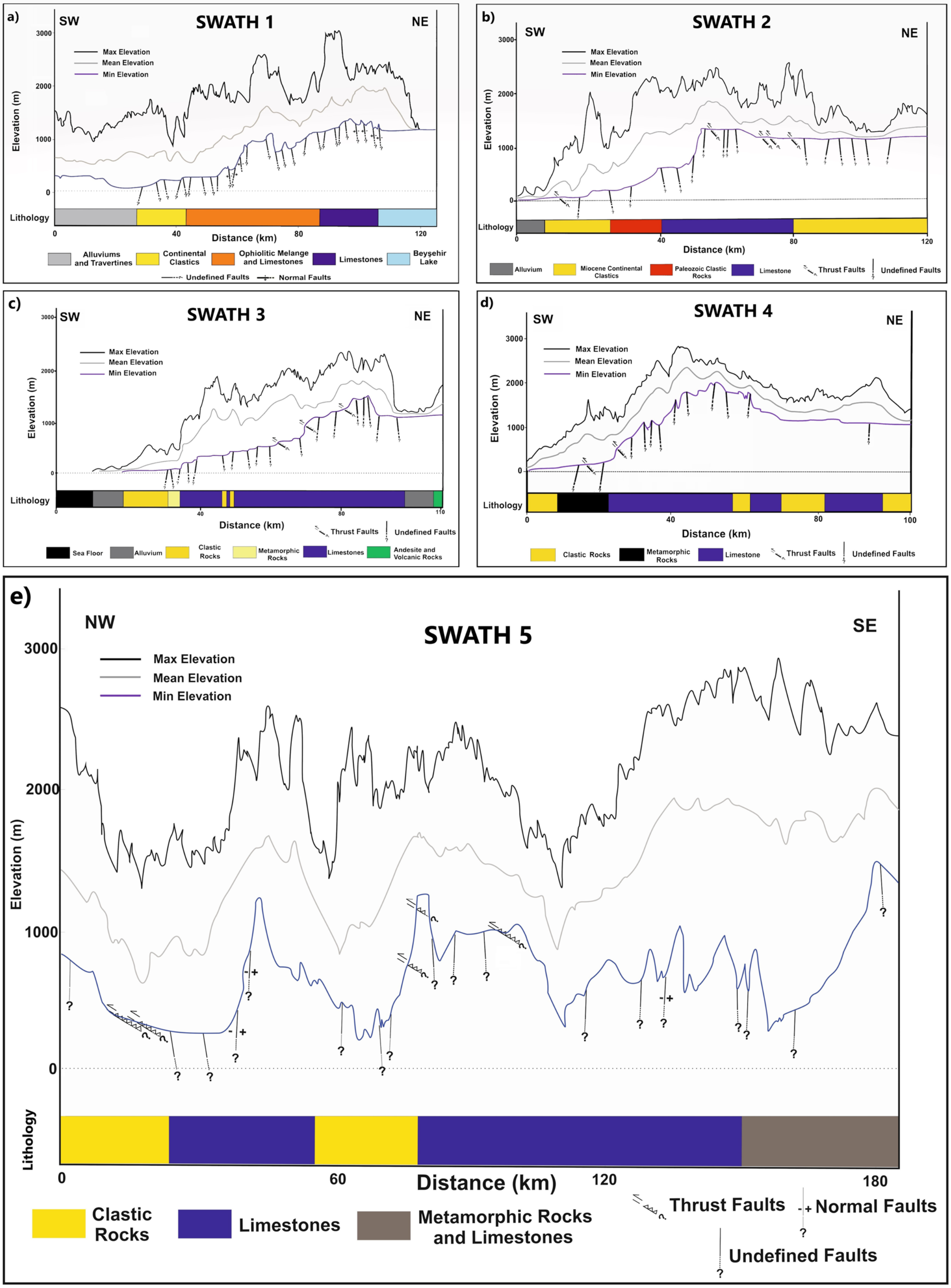

Figure 2. (a–d) Topographical swath profiles orthogonal to the Central Taurides (CT). (e) Topographical swath profile parallel to the CT. Swath profile footprints are given in Figure 1c. The color bars under the profiles are lithological classes; legends are given in each profile.

10.1029/2022TC007550

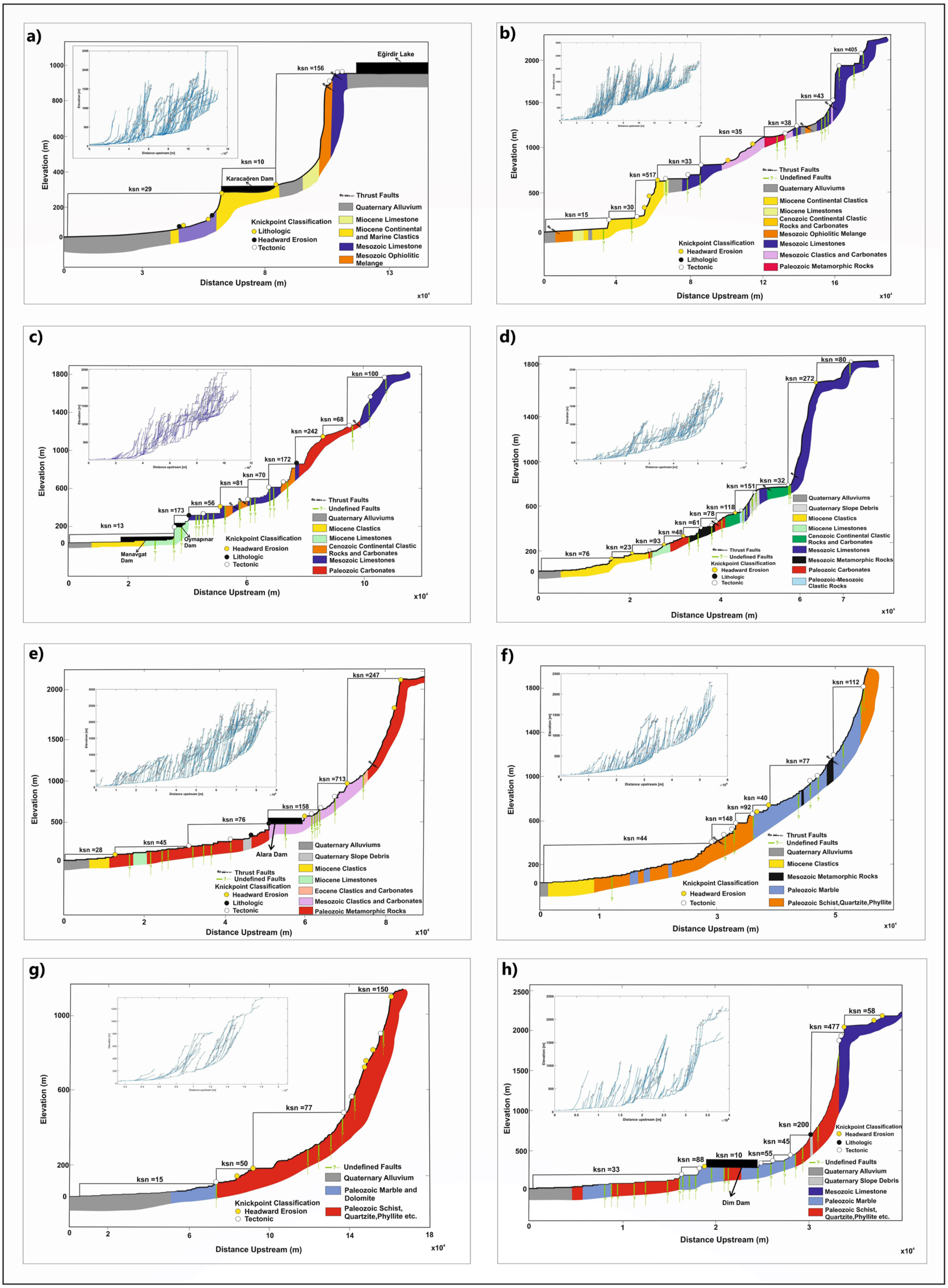

Figure 3. Longitudinal topographic and geologic profiles, knickpoint classification, and ksn values of the channel segments along the trunk rivers. Knickpoint classification is based on slope-area plots and spatial relationship between lithology, faults, and river trunks. The legend of the geological features and knickpoints are given within the figures. All knickpoints and longitudinal profiles within river basins presented as inlets. (a) Aksu River, (b) Köprüçay River, (c) Manavgat River, (d) Karpuzçay River, (e) Ulugüney River, (f) Kargı River, (g) Oba River, and (h) Dim River. Please note that horizontal and vertical scales are different for each profile.

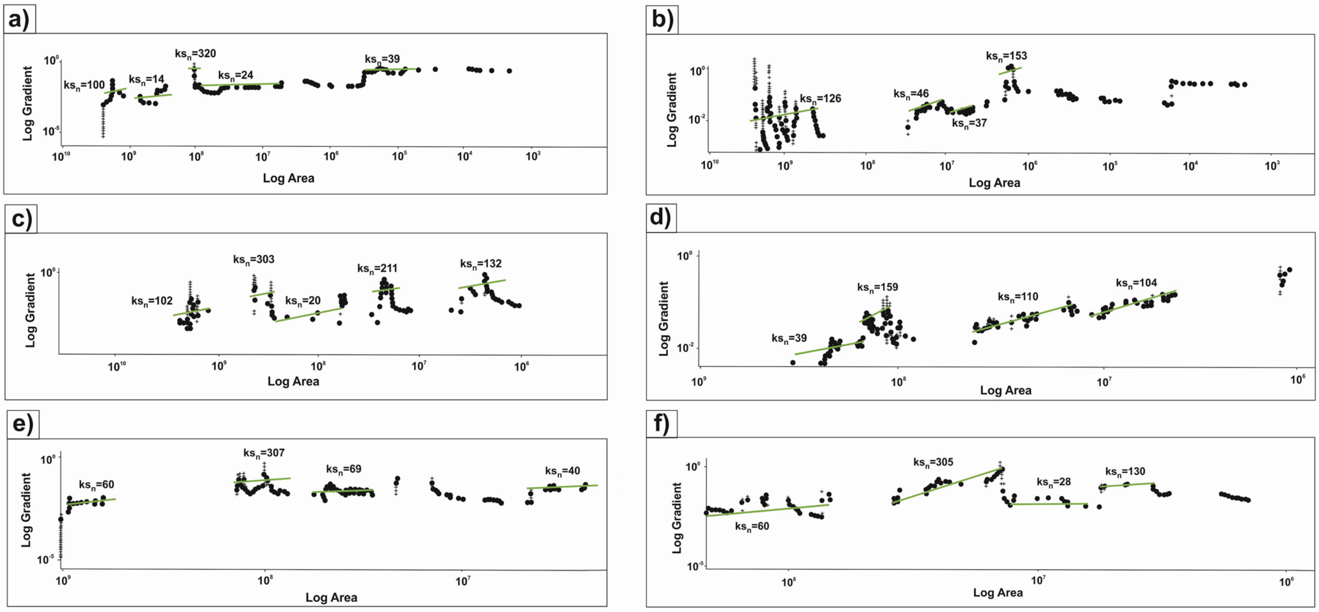

Figure 4. Slope-area plots of the trunk streams in log-log space. Green lines are regression lines of the best-fit ksn values of the channel segments. (a) Aksu River, (b) Köprüçay River, (c) Manavgat River, (d) Kargı River, (e) Ulugüney River, and (f) Dim River.

4.3. Topographical Relief Analysis and Surface Uplift Estimates

The relief or the erosion depth is 1,689 m between the valley bottoms and ridge tops across the flank (Figure 7). Low relief areas are mostly distributed along the Antalya and Beyşehir-Suğla basins, approximately between 0 and 1,000 m elevations. The high relief areas are clustered at the middle part, and the southeastern part of the flank, and they correspond to the upthrown blocks of the Aksu, Kırkkavak and the major fault zones. The high relief areas mainly underlain by relatively resistant lithological units like Mesozoic limestones and Paleozoic metamorphic rocks (Figure 1d). The local topographical relief gradually increases from the western to the eastern parts, from the Aksu River Basin to the Dim River Basin across the flank. The low relief upland surfaces are scattered but continuous across western CT. The relic upland surfaces are usually found as bounded by normal faults and further fragmented by the extensional active tectonics. These surfaces are distributed roughly between 400 and 2,600 m and clustered around 2,000 m elevations mostly in the mountainous part of western CT. The elevations of these surfaces are higher in the eastern part of the study area. The elevation of the slope-break knickpoints that bound the upland surfaces also increases from 1,700 to 1,800 m in the west to 2,000–2,100 m in the east (Figure 5c).

Using the spatial extent and the modern elevation of the low relief upland surfaces, we estimated the long-term vertical deformation and amount and the pattern of the surface uplift throughout the flank. We selected five bedrock streams (Köprüçay, Manavgat, Karpuzçay, Ulugüney, and Dim Rivers) that are sourcing from perched low relief surfaces. We calculated surface uplift as 1,600 ± 50 m from Köprüçay River, 1,650 ± 50 m from Manavgat River, 1,700 ± 50 m from Karpuzçay River, and 1,800 ± 50 m from Ulugüney and Dim rivers. The mean surface uplift is 1,710 ± 50 m and the surface uplift tends to increase from west to east, from 1,600 ± 50 to 1,800 ± 50 m (Figures 5 and 6).

Monod et al. (2006) dated the relic upland surfaces to Early-Middle Miocene according to the age of the paleo-fluvial system, which they inferred from the conglomerates interfingering with Langhian marine sediments found within a paleo valley (İncebel Valley). However, according to robust evidence from former studies, the surface uplift is post-Tortonian (<8 Ma) based on Tortonian Marine Sediments in western and CT (Cosentino et al., 2012; Radeff et al., 2017; Schildgen et al., 2012a, 2012b, 2014).

4.4. Kinematic Measurements and Paleo-Stress Analysis

We conducted kinematic measurements on fault planes along fault zones at six key areas between Manavgat and Seydişehir from coast to plateau. Most of the fault planes have clear slickenlines, slicken fibers and polished

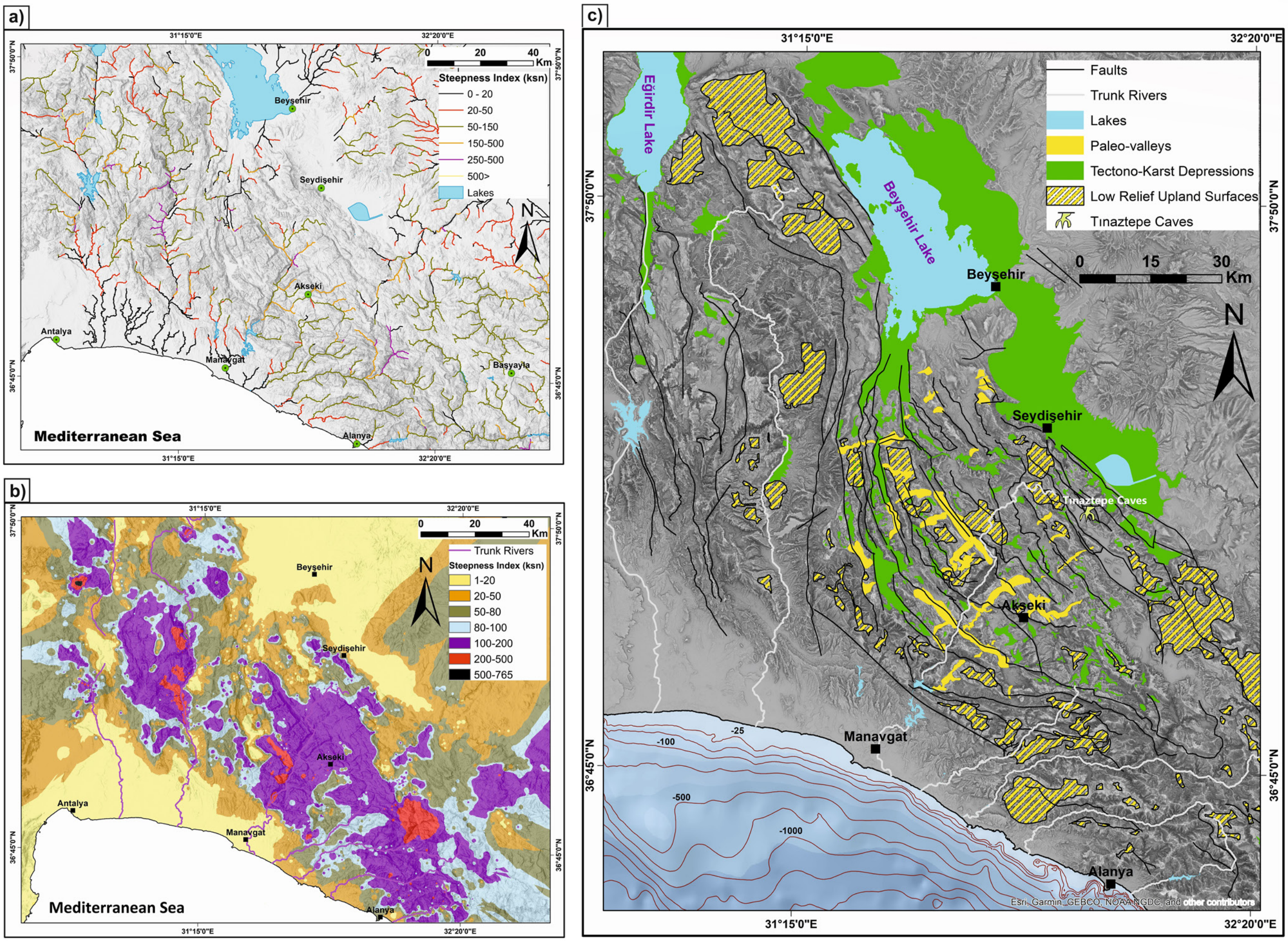

Figure 5. (a) The best-fit ksn values of the main stream channels. (b) The distribution of the ksn values produced by the inverse distance weighting interpolation. (c) Spatial distribution of the low relief upland surfaces, paleo-valleys and tectono-karst depressions. Paleo-valleys are from Monod et al. (2006). Bathymetry data is from GEBCO (The General Bathymetric Chart of the Oceans) (https://www.gebco.net).

surfaces. We observed vertical striations characterizing pure normal and oblique movements along the major fault zones. We also observed horizontal slickenlines that demonstrate strike-slip movements, especially in the relatively minor secondary deformation zones (Figures 8c and 8f).

Location c is found near Huğlu in the northwestern part of the study area. Here, the fault planes are relatively small and present secondary structures that are oblique to a broad NW-SE striking fault zone. We observed near-horizontal striations that show mainly left lateral strike-slip movements. We also found near-horizontal slickenlines that show mainly right-lateral strike-slip movements at Location f. This location is found near the Yarpuz and also corresponds to a small-scale secondary lineation. The paleo-stress analysis shows NE-SW extension and NW-SE compression directions, and the stress ratio (R) values demonstrate pure strike-slip deformation type at Locations c and f. Locations a, b, d, and e correspond to NW-SE striking main fault zones. The slickenlines and slicken fibers demonstrate normal faulting at all four locations. Analysis of the fault-slip data characterizes a NE-SW extensional stress regime and the "R" values of 0.50, 0.48, and 0.40 denote pure extensional deformation type (Figure 8).

5. Discussion

5.1. Implications for Regional Active Deformation Pattern

Our geomorphic outputs point out to an actively deforming transient landscape and changing deformation patterns across western CT (Figure 6). Downstream increases in the channel steepness values and major slope-break

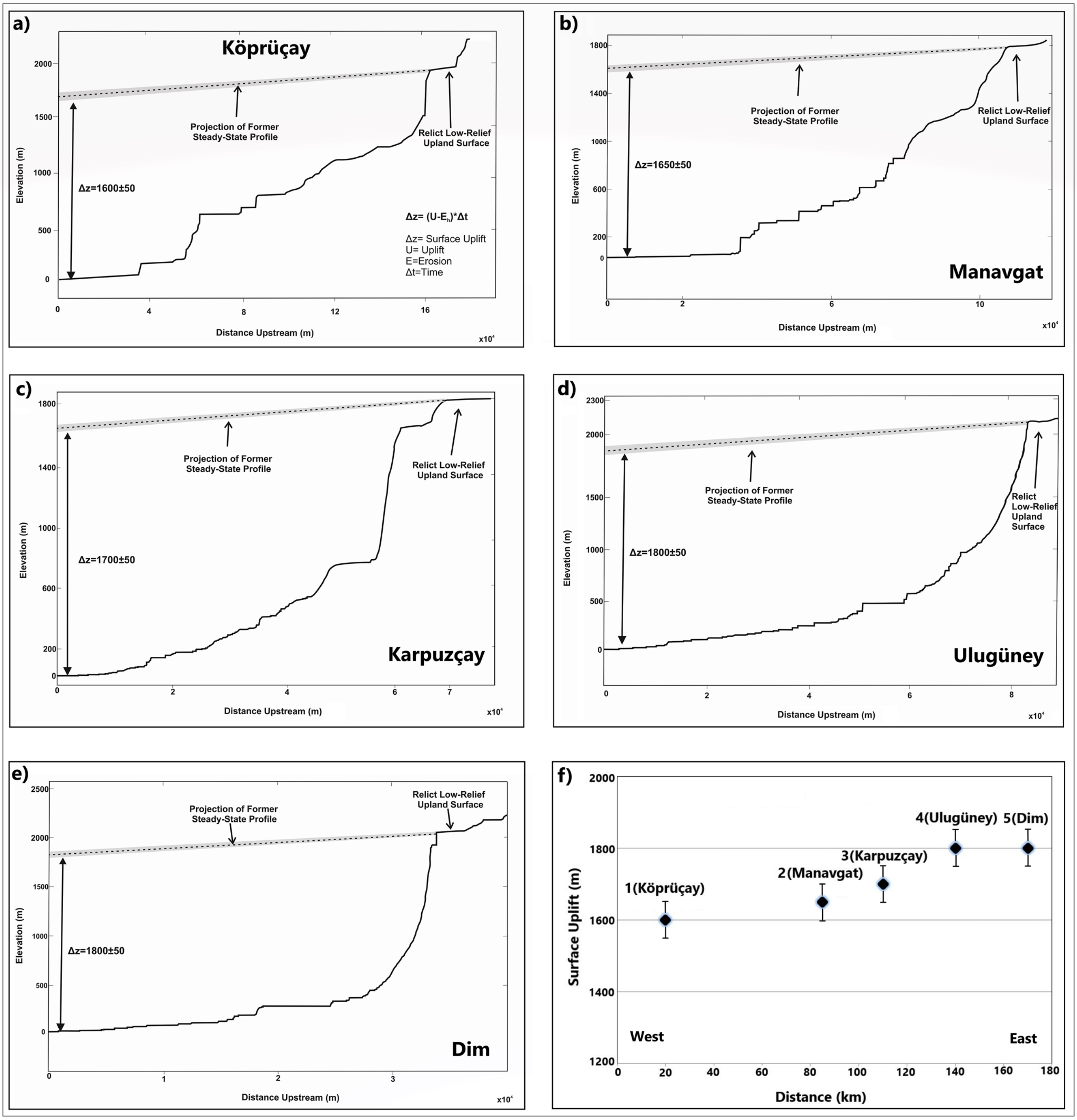

Figure 6. (a–e). Current and projected relic longitudinal profiles of the bedrock rivers that are sourcing from the relict low relief upland surfaces. Concepts and the equation (given in (a)) for calculating surface uplift is from Kirby and Whipple (2012). (a) Köprüçay River, (b) Manavgat River, (c) Karpuzçay River, (d) Ulugüney River, (e) Dim River. (f) Scatter plot of the surface uplift pattern; from the western part, Köprüçay River basin to the eastern part, Dim River basin. Numbers (1–5) present the location of the rivers given in Figure 7.

tectonic knickzones demonstrate different uplift pulses or periods of intensifying deformation. The ksn values demonstrate a bell-shaped trend in the north-south direction, and the best-fit ksn reaches peak values along the mountainous zone of the CT. The cumulative surface uplift slightly increases from west to east, from 1,600 ± 50 to 1,800 ± 50 m. The increasing trend of the ksn values, more rugged topography and more evident slope-break knickzones in the longitudinal profiles provide further morphometric evidence of the intensifying deformation toward the eastern parts of western CT. Results of the previous studies also mentioned a trend of increasing

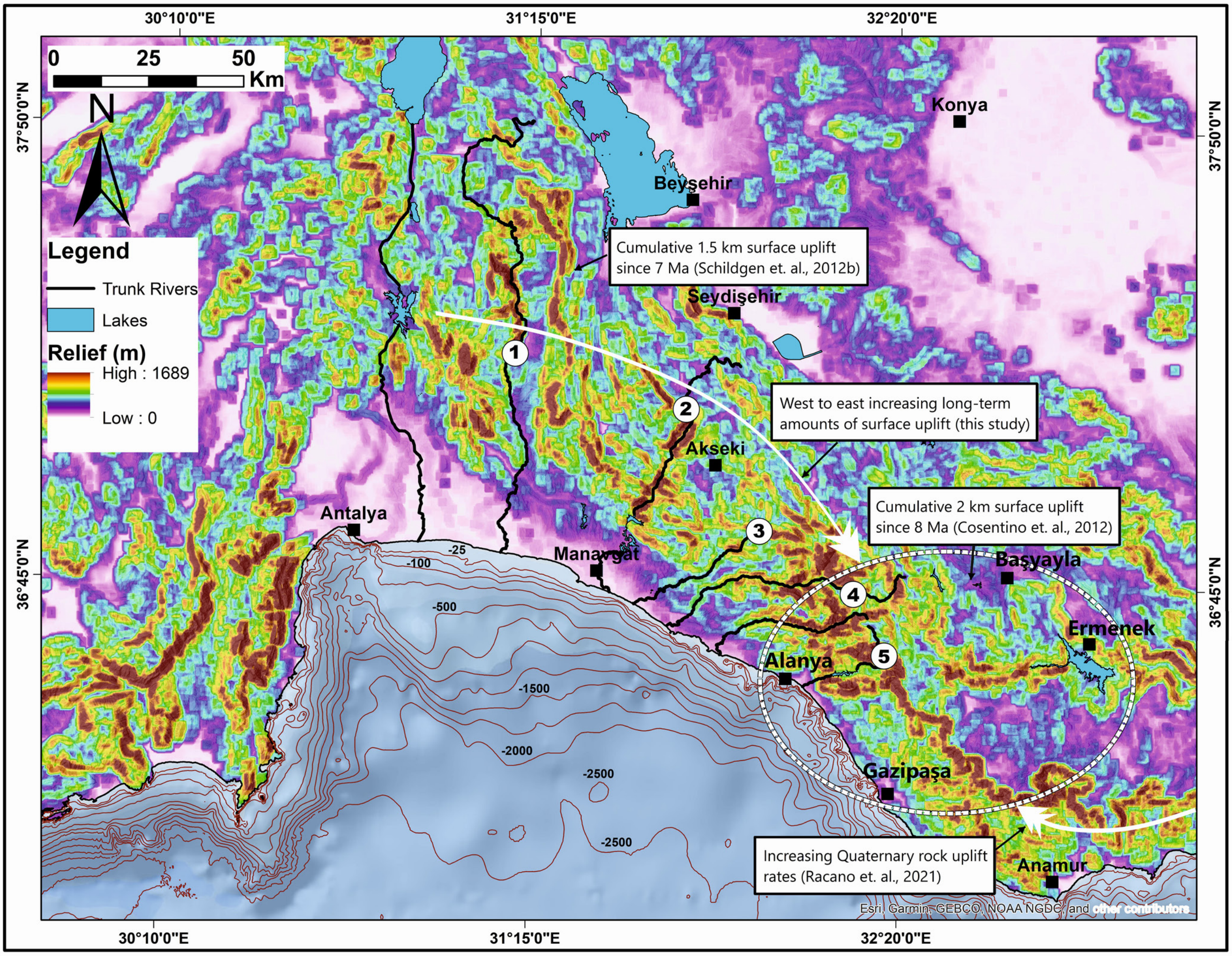

Figure 7. The general topographic relief across the western flank of the Central Taurides (CT). The white arrows show the cumulative uplift trend of our results and the Quaternary rock uplift trend from Racano et al. (2021). The numbers within the white boxes depict the trunk rivers that have been used in paleo-longitudinal profile projection analysis: 1—Köprüçay River, 2—Manavgat River, 3—Karpuzçay River, 4—Ulugüney River, 5—Dim River. Data from the previous studies have been briefly given within the white boxes for interpreting the spatial distribution of the uplift. The white circle represents our proposed maximum uplift zone across the CT. Please note that the uplift trend is compatible with the relief character.

cumulative uplift from the western to the eastern flank of the CT for the last 8 Ma (Cosentino et al., 2012; Schildgen et al., 2012a, 2014) and an increasing Quaternary rock uplift rate from the eastern flank toward the western flank of the CT (Racano et al., 2021) (Figure 7). Integration of our results with findings of previous studies suggests a differential uplift pattern in the west-east direction across the southern margin that reaches up to maximum values in the region of Alanya-Başyayla-Ermenek-Gazipaşa, with a gradually decreasing pattern from this region toward the eastern and western parts of the CT (Figure 7).

The studies show that the stress states and spatial distribution of the crustal deformation are diverse across the undergoing African Plate, subduction interface and overriding Anatolian Plate across the Eastern Mediterranean. The undergoing African Plate and subduction interface mostly deforming by aseismic processes, and the deep-rooted reverse and strike-slip earthquake focal mechanisms indicate that the infrequent brittle deformation is mostly contractional (Howell et al., 2017; Robertson, 1998; Wdowinski et al., 2006). Contrary to ongoing contraction along the Cyprus trench, the extensional tectonic deformation prevails on the overriding Anatolian Plate.

The upper crust of western CT is seismically very active and the shallow earthquake focal mechanism solutions suggesting that upper crustal extension and normal faulting is active today (Figures 1d and 9a). Several studies also provided evidence for normal and transtensional faulting between the Pliocene and Recent times in the

10.1029/2022TC007550

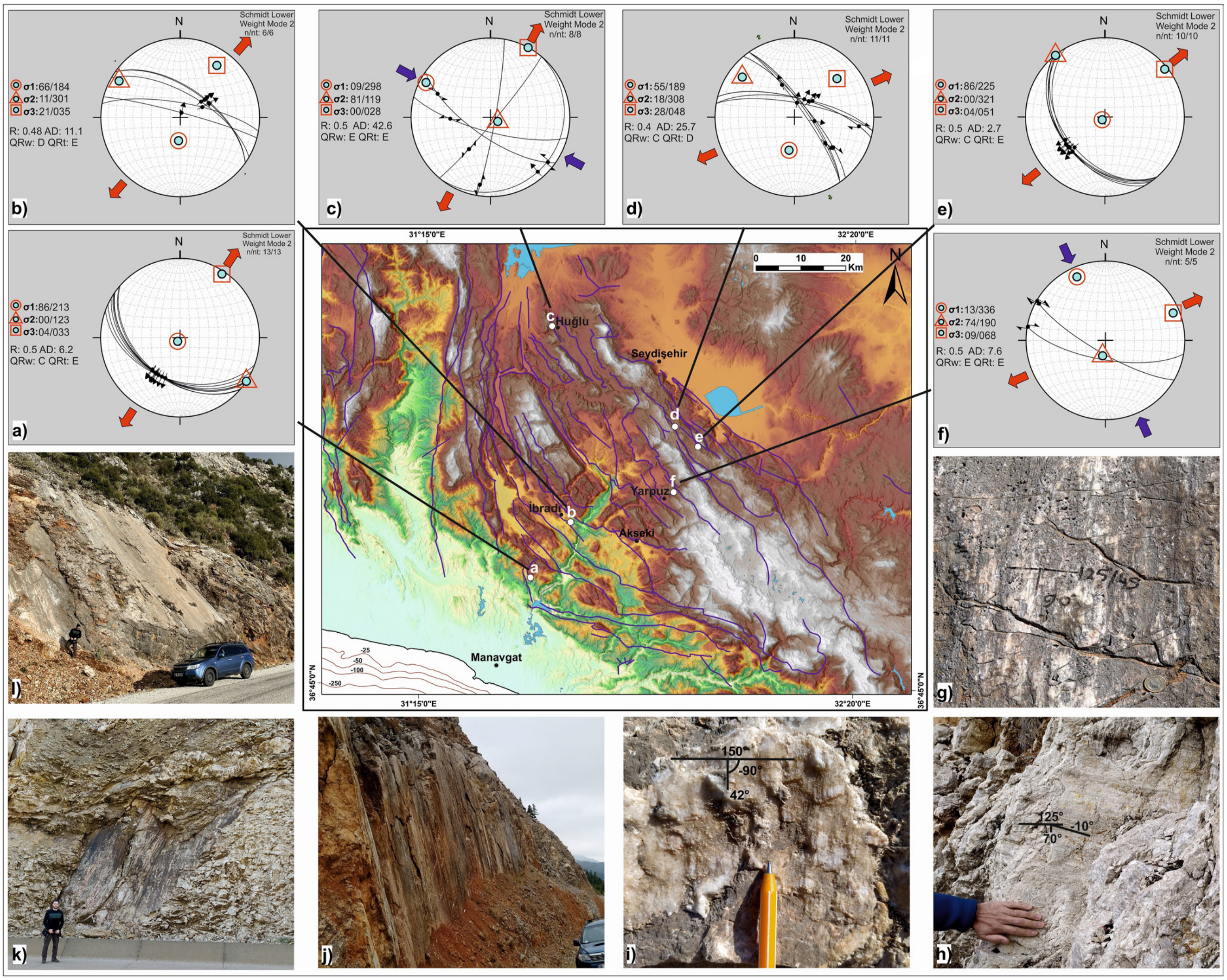

Figure 8. (a–f) Plotted results of kinematic analysis. Measurement locations are shown on the map with white circles. Please note that red and blue arrows demonstrate extension and compression directions respectively. (g) Slickenlines and calcite fibers showing the pure extensional deformation at location a. (h) Slickenlines showing the sinistral movement at location c. (i) Calcite fibers showing the pure extensional deformation at Location e. (j) General view of fault plane at location d. (k) General view of fault plane at location b. (l) General view of fault plane at location a. Please note that the strike, dip angle and rake values of fault planes are given in photos (g–j).

northeastern margin of the Isparta Angle (Emre et al., 2003; Koçyigit & Özacar, 2003), in the Aksu Basin (Glover & Robertson, 1998b; Üner et al., 2015), along the Kırkkavak Fault (Schildgen et al., 2012b) and in the Antalya Bay (Glover & Robertson, 1998a) across the southwestern Anatolia. GPS-derived strain-rate fields of Howell et al. (2017), also provides more evidence for recent upper crustal extensional deformation in western CT. Our kinematic analyses are in agreement with the current earthquake data, and provide further evidence for the last phase of brittle deformation across the western CT. Our kinematic measurements along the main undefined faults have yielded a systematic NE-SW extensional deformation across a broad zone between Manavgat-Seydişehir. The focal mechanisms of the modern shallow earthquakes and pseudo-fault mechanisms based on our kinematic measurements all show that the youngest generation of deformation compensated along the NW-SE oriented major normal fault zones and N-S and NE-SW oriented relatively small-scale strike-slip fault systems (Figure 8). Kinematic results and pseudo-fault mechanisms of Üner et al. (2015) within the Aksu Basin and Schildgen et al. (2012b) along the Kırkkavak Fault shows that the NE-SW extensional stress regime is continuous across the western flank of the CT (Figure 9a).

Tectono-karst footprints and morphotectonic expressions of the active tectonic deformation are highly prominent across western CT. The long-term cumulative mean 1,710 ± 50 m surface uplift (Figure 6) that has accelerated in the Pleistocene (Öğretmen et al., 2018; Schildgen et al., 2014) possibly triggered the intense karstification and

10.1029/2022TC007550

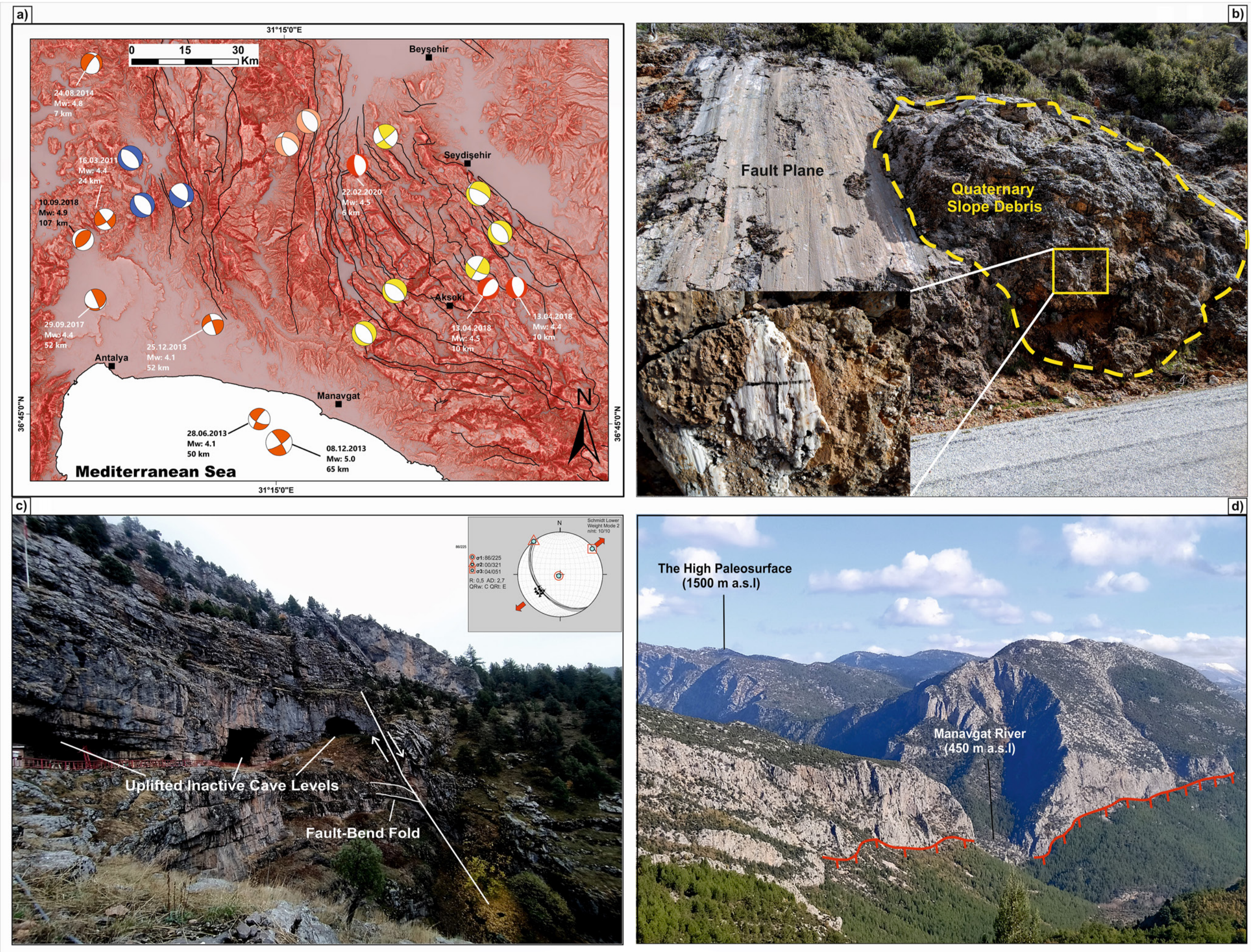

Figure 9. (a) Red Relief Image Maps with the modern earthquake focal mechanisms (colored red) and pseudo-focal mechanisms derived from the inversion modeling based on the kinematic indicators of the youngest generation of the brittle structures. Pseudo-fault mechanisms colored yellow are produced according to our kinematic measurements (Figure 8). Green-colored mechanisms are from Schildgen et al. (2012b), blue colored mechanisms are from Üner et al. (2015). Black lines are the main faults of Şenel (2002). Focal mechanism solutions are from Boğaziçi University-Kandilli Observatory and Earthquake Research Institute (http://www.koeri.boun.edu.tr/sismo/2/moment-tensor-solutions/) and Disaster and Emergency Management of Turkey (AFAD) (https://deprem.afad.gov.tr/faycozumleri?lang=en). (b) Quaternary slope debris amalgamated onto the fault plane at location a. Inlet shows that it has been cut by the faults' activity. (c) Normal fault cutting the entrance of the Tınaztepe Caves in the southeast of the Seydişehir. The inlet graph is the result of the paleo-stress analysis given in Figure 8e; measurements made in the 1 km southeast of the cave entrance which corresponds to the kinematically continuous part of the fault. The location of the Tınaztepe Caves is given in Figure 5c. (d) Relief bounding undefined normal fault with very characteristic triangular facets near İbradı. The high paleosurface located at 1,500 m elevation (Monod et al., 2006) demonstrates an approximately 1,050 m bedrock incision of Manavgat River.

gradual lowering of the karst base level; hence the formation of the polycyclic and polygenetic karst landforms. For example, abandoned three levels of Tınaztepe Cave can be found southeast of Seydişehir. Effects of the recent extensional tectonics can be seen as well, as an undefined normal fault cuts the cave entrance and compensates the uplift of the Tınaztepe Ridge block and the formation of two inactive cave levels at the 1,500 and 1,533 m elevations (Figure 9b). Reactivation of the thrust zones as normal faults with clear geomorphic expressions is also widespread across the flank. For example, an inherited thrust zone (Akay & Uysal, 1988; McPhee et al., 2018) that reactivated as a normal fault bound the deeply incised Üzümdere Gorge of the Manavgat River near İbradı (Figure 9c). These normal fault bounded-deeply incised valleys are widespread in the upper reaches of all bedrock streams, implying the young uplift of the western CT and high incision of the river system. The effects of the active deformation are evident on geomorphological orientations as well; NW-SE striking tectono-karst depressions (such as Eynif and Kembos Poljes) and horst-graben structures is compatible with the orientations of the youngest fault generations and active NE-SW extension. Our results show that the surface uplift and the active extensional deformation significantly controlled the morpho-tectonic development in western CT (Figure 10).

10.1029/2022TC007550

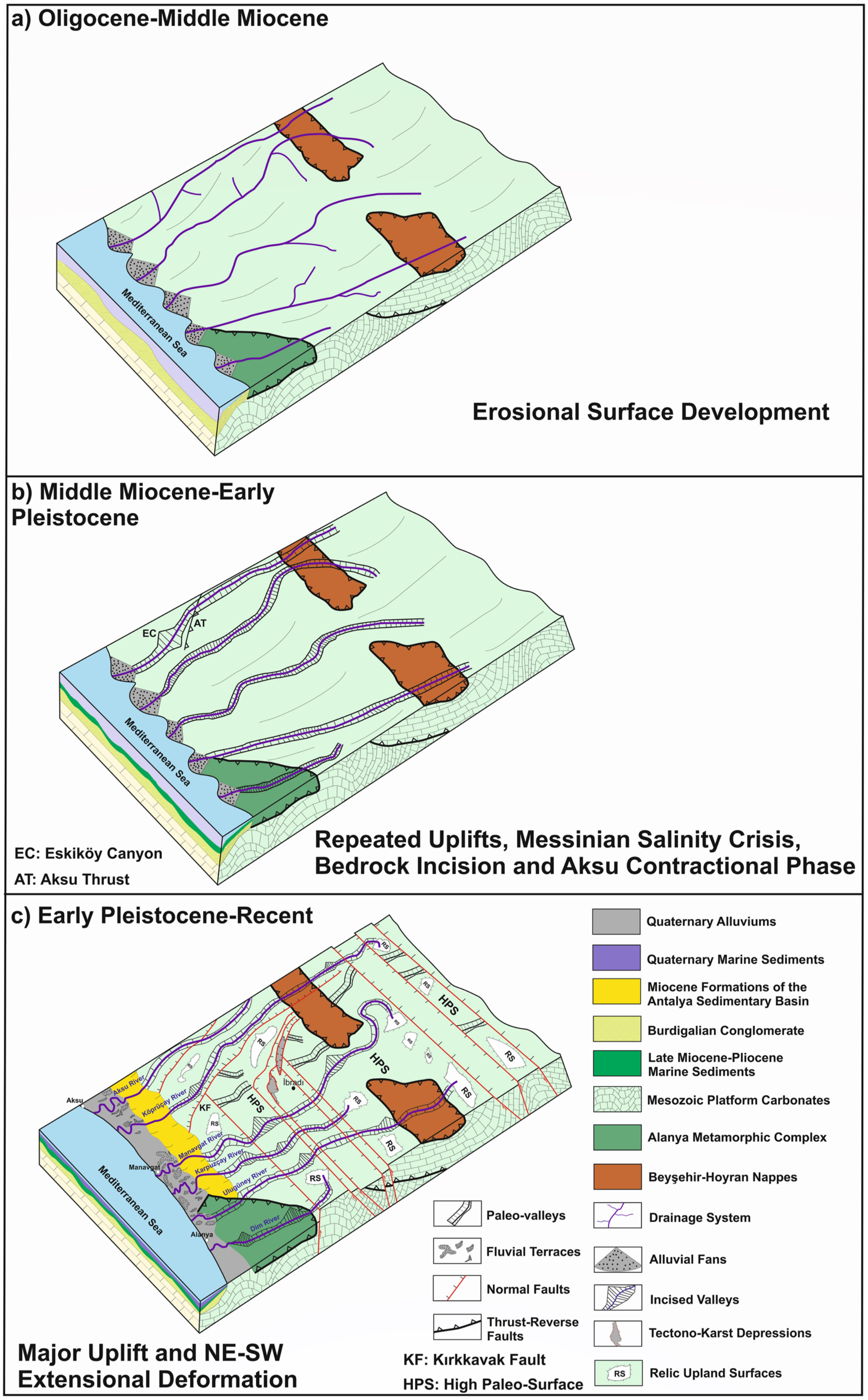

Figure 10. A conceptual model for the western flank of the Central Taurides, which depicts the pattern of deformation between Oligocene-Recent. Please note that layers of "Late Miocene-Pliocene Marine Sediments" and "Quaternary Marine Sediments" are tentative.

10.1029/2022TC007550

Although the westernmost CT (Aksu Basin) has been under the influence of active extensional deformation since the Late Pliocene (Glover & Robertson, 1998b; Üner et al., 2015), our results suggest that the earlier contractional Aksu Phase had effects on the evolution of the topography and the patterns of deformation. Higher ksn values and tectonic knickpoints across the hanging walls of the thrust faults underline the effects of the “Aksu Phase” on the topography. The contractional deformation also controlled the orientation of the main tectonic lineaments and prepared the groundwork for the development of N-S striking extensional morphotectonic features (like Kovada Graben). Thus, although the last extensional deformation phase mainly controlled the geomorphological development in the westernmost CT, our findings suggest that the Aksu Phases' contractional deformation also had significant effects on the shaping of the topography.

5.2. Implications for Driving Forces

The surface uplift and active deformation of the CT have long been associated with the complex mantle processes related to subduction and slab deformation (Cosentino et al., 2012; Facenna et al., 2013; McPhee et al., 2022; Öğretmen et al., 2018; Racano et al., 2021; Schildgen et al., 2012a, 2012b, 2014). To investigate the properties of the mantle and the geometries of the slabs under the Eastern Mediterranean, comprehensive geophysical studies have been carried out in the last two decades. While there is no slab seen under the east of Cyprus, there is geophysical evidence showing the segmentation of the subducting Cyprus slab into two separate fragments known as the western Cyprus slab (or Antalya Slab) and eastern Cyprus slab (Biryol et al., 2011; Güvercin et al., 2021; Portner et al., 2018). These two slab fragments separated from one another with the Paphos Transform Fault (Figure 1a). Tomographic imaging data (Biryol et al., 2011; Facenna et al., 2006; Kounoudis et al., 2020; Portner et al., 2018) also detected slow velocity anomalies that were interpreted as vertically rising asthenosphere through the slab tears under Southern Turkey. Considering the extensive geophysical evidence on the slab deformation; the west to the east increasing cumulative surface uplift pattern in the western CT and the dome-like active uplift pattern across the CT can be explained by asthenospheric upwelling through the torn/broken slab window between the Antalya slab and eastern Cyprus slab, as the peak amounts and rates of uplift are found here.

What driving process (es) control the active extensional brittle deformation in the western CT? Schildgen et al. (2012b) and Howell et al. (2017) proposed that extensional deformation is related to warming and relaxation of the crust as a consequence of slab deformation and following asthenosphere upwelling processes. Considering the changing directions of the extension on a regional scale across southern Turkey (E-W, N-S, NW-SE, and NE-SW) (Howell et al., 2017), this process may be considered the dominant driving mechanism of the extensional deformation across Southern Turkey. On the other hand, many studies related the Quaternary extensional regime to a subduction and slab roll-back of a relic remnant of the southern Neo-Tethys Ocean (Flecker et al., 2005; Glover & Robertson, 1998b; Kelling et al., 2005; Koçyigit & Özacar, 2003; Üner et al., 2015), and the new geophysical evidence points out ongoing subduction in the west of Cyprus. Biryol et al. (2011) suggested that the current location of the slab in western Cyprus implies that the slab rolled southwards between the Early Miocene and the Present. Furthermore, it has been recently suggested that the Antalya Slab is continuously subducting toward NE, under the western CT and poses a similar geometry to the Aegean slab according to the new focal mechanisms catalog (Güvercin et al., 2021) and newly updated P-wave tomography data (Portner et al., 2018). Does (Did?) the SW retreat of Antalya slab contribute to the NE-SW extension across the western CT? Compensation of the brittle extensional deformation along the NW-SE striking reactivated thrust and overthrust weakness zones, complicates our understanding of the extent of the underlying causes of the NE-SW extension in the western CT, whether it is caused by the crustal relaxation or the slab retreat, or both.

The most evident difference between the western flank and other parts (central and eastern) of the southern margin is the presence of denser crustal deformation (faulting). The western flank has the highest fault density along the southern margin, and it creates the coarsest topographic texture (the most dissected). While the surface uplift in the east of our study area and western CT is possibly controlled by the slab deformation and asthenospheric upwelling, brittle deformation and reactivation of the paleotectonic weakness zones can be attributed to some kind of combination of the rollback of the Antalya slab and relaxation of the crust in the neotectonic period. The Aksu Phase especially affected the deformation of the westernmost part of the CT in between the Late Miocene and the Late Pliocene and created the contractional structures possibly related to counter-clockwise rotation of the Anatolian Plate (Çiner et al., 2008) or convergence along the Cyprus Trench (McPhee et al., 2018) in Southwest Anatolia. This deformation controlled the development of the N-S oriented tectonic lineaments and morphotectonic units at the westernmost part of the CT. Tearing and probably breaking of the Cyprus slab at the west of Cyprus following the arrival of the Eratosthenes Seamount at the Cyprus Trench in Pliocene-Pleistocene transition (Robertson, 1998; Schattner, 2010), may contributed to differential uplift across the CT with a localized dome-like uplift pattern peaking at the Alanya-Başyayla-Ermenek-Gazipaşa region. This dome-like uplift seems to be still active according to current GPS data (Serpelloni et al., 2013) and Holocene sea-level markers (Cosentino et al., 2016; Kelletat & Kayan, 1983; Liberatore et al., 2022). Related asthenospheric upwelling through the torn/broken slab presumably caused the crustal relaxation and contributed to the extensional active deformation along the paleotectonic weakness zones throughout the Quaternary. While all these suggestions are theoretically valid, elucidating the extent of the driving mechanisms requires further geochronological constraints on the brittle deformation, seismic activity and morphotectonic evolution in the western flank of the CT.

6. Conclusions

New geomorphic data from western CT revealed the existence of the major tectonic slope-break knickzones and steep channel segments along the river longitudinal profiles, strong relief contrasts that reflects the signals of the crustal deformation recorded within the post-orogenic transient actively deforming topography. The spatial distribution of the low relief upland surfaces constrained the long-term surface uplift pattern; the mean cumulative surface uplift is 1,710 ± 50 m, and shows an increasing trend from west to the east, from 1,600 ± 50 to 1,800 ± 50 m. Distributions of the best-fit ksn values, relief ruggedness, and slope-break tectonic knickzone elevations point out an increasing deformation intensity toward the eastern CT. Integration of our results with findings of the previous studies suggests a dome-like uplift pattern that reaches up to maximum values in the region of Alanya-Başyayla-Ermenek-Gazipaşa, with a gradually decreasing pattern from this region toward the eastern and western flanks of the CT. Our kinematic measurements along the main faults revealed a systematic NE-SW active extensional deformation across a broad 200 km zone between Manavgat-Seydişehir from coast to the plateau. The youngest brittle deformation compensated along the NW-SE oriented major normal fault zones and N-S and NE-SW oriented relatively small-scale strike-slip fault systems. The active deformation in the western flank of the CT can be related to both mantle and crustal processes. While the surface uplift of the western CT is possibly controlled by the slab fragmentation and hot asthenosphere upwelling, the driving mechanisms for the NE-SW extension is probably a combination of slab-rollback and crustal relaxation processes. Aksu Phase also affected the orientation of the main tectonic lineaments and the morphotectonic features in the westernmost CT. The results of this study decipher the long-term surface uplift pattern between Antalya-Alanya and kinematic features of the youngest brittle deformation for the first time between Seydişehir-Manavgat. Our findings have significant implications for understanding the morphotectonic development and post-orogenic deformation in the plateau margins, and geodynamic evolution of the Eastern Mediterranean.

Data Availability Statement

Digital elevation models used in this study are open-access and obtained from "https://earthexplorer.usgs.gov" and "https://asf.alaska.edu/." All the other data used in this study can be obtained in the figures and references (ALOS PALSAR Radiometric Terrain Corrected High Resolution, 2015; NASA Shuttle Radar, 2013).

Acknowledgments
This study was funded by the Scientific and Technological Research Council of Turkey (Grant TUBITAK 118C275 to I.T. Uysal).

References

Akay, E., & Uysal, S. (1988). Post-Eocene tectonics of the Central Taurus Mountains. *Mineral Resources Exploration Bulletin*, *108*, 23–34.

Allmendinger, R. W., Jordan, T. E., Kay, S. M., & Isacks, B. L. (1997). The evolution of the Altiplano-Puna plateau of the Central Andes. *Annual Review of Earth and Planetary Sciences*, *25*(1), 139–174. https://doi.org/10.1146/annurev.earth.25.1.139

ALOS PALSAR Radiometric Terrain Corrected High Resolution. (2015). Dataset: ASF DAAC, includes material © JAXA/METI 2007 [Dataset]. https://doi.org/10.5067/Z97HFCNKR6VA

Biryol, B. C., Beck, S. L., Zandt, G., & Özacar, A. A. (2011). Segmented African lithosphere beneath the Anatolian region inferred from teleseismic P-wave tomography. *Geophysical Journal International*, *184*(3), 1037–1057. https://doi.org/10.1111/j.1365-246X.2010.04910.x

Boulton, S. J. (2020). Geomorphic response to differential uplift: River long profiles and knickpoints from Guadalcanal and Makira (Solomon Islands). *Frontiers of Earth Science*, *8*. https://doi.org/10.3389/feart.2020.00010

Chen, Y. W., Shyu, J. B. H., & Chang, C. P. (2015). Neotectonic characteristics along the eastern flank of the Central Range in the active Taiwan orogen inferred from fluvial channel morphology. *Tectonics*, *34*(10), 2249–2270. https://doi.org/10.1002/2014TC003795

Cheng, F., Garzione, C. N., Mitra, G., Jolivet, M., Guo, Z., Lu, H., et al. (2019). The interplay between climate and tectonics during the upward and outward growth of the Qilian Shan orogenic wedge, northern Tibetan Plateau. *Earth-Science Reviews*, *198*, 102945. https://doi.org/10.1016/j.earscirev.2019.102945

Chiba, T., Kaneta, S., & Suzuki, Y. (2008). Red relief image map: New visualization method for three dimensional data. In *The International Archives of the Photogrammetry, Remote Sensing and Spatial Information Sciences*, (Vol. 37, pp. 1071–1076).

Çiner, A., Doğan, U., Yıldırım, C., Akçar, N., Ivy-Ochs, S., Alfimov, V., et al. (2015). Quaternary uplift rates of the Central Anatolia Plateau, Turkey: Insights from cosmogenic isochron-burial nuclide dating of the Kizilirmak River terraces. *Quaternary Science Reviews*, *107*, 81–97. https://doi.org/10.1016/j.quascirev.2014.10.007

Çiner, A., Karabiyikoǧlu, M., Monod, O., Deynoux, M., & Tuzcu, S. (2008). Late Cenozoic sedimentary evolution of the Antalya Basin, southern Turkey. *Turkish Journal of Earth Sciences*, *17*(1), 1–41.

Clark, M. K., Royden, L. H., Whipple, K. X., Burchfiel, B. C., Zhang, X., & Tang, W. (2006). Use of a regional, relict landscape to measure vertical deformation of the eastern Tibetan Plateau. *Journal of Geophysical Research*, *111*(F3), F03002. https://doi.org/10.1029/2005JF000294

Cosentino, D., Ögretmen, N., Cipollari, P., Gliozzi, E., Radeff, G., & Yildirim, C. (2016). Evidence for latest Pleistocene to Holocene uplift at the southern margin of the Central Anatolian Plateau (CAP), southern Turkey. *EGU General Assembly Conference Abstracts 2016* (p. EPSC2016-8873).

Cosentino, D., Schildgen, T. F., Cipollari, P., Faranda, C., Gliozzi, E., Hudáčková, N., et al. (2012). Late Miocene surface uplift of the southern margin of the Central Anatolian plateau, Central Taurides, Turkey. *Bulletin of the Geological Society of America*, *124*(1–2), 133–145. https://doi.org/10.1130/B30466.1

Cyr, A. J., Granger, D. E., Olivetti, V., & Molin, P. (2010). Quantifying rock uplift rates using channel steepness and cosmogenic nuclide-determined erosion rates: Examples from northern and southern Italy. *Lithosphere*, *2*(3), 188–198. https://doi.org/10.1130/L96.1

Delvaux, D., & Sperner, B. (2003). New aspects of tectonic stress inversion with reference to the TENSOR program. *Geological Society London Special Publications*, *212*(1), 75–100. https://doi.org/10.1144/GSL.SP.2003.212.01.06

Demoulin, A., Beckers, A., Rixhon, G., Braucher, R., Bourles, D., Siame, L., & Becker, A. (2012). Valley downcutting in the Ardennes (W Europe): Interplay between tectonically triggered regressive erosion and climatic cyclicity. *Netherlands Journal of Geosciences*, *91*(1–2), 79–90. https://doi.org/10.1017/S0016774600001517

Demoulin, A., Mather, A., & Whittaker, A. (2017). Fluvial archives, a valuable record of vertical crustal deformation. *Quaternary Science Reviews*, *166*, 10–37. https://doi.org/10.1016/j.quascirev.2016.11.011

Doğan, U., Koçyiğit, A., & Gökkaya, E. (2017). Development of the Kembos and Eynif structural poljes: Morphotectonic evolution of the upper Manavgat River basin, Central Taurides, Turkey. *Geomorphology*, *278*, 105–120. https://doi.org/10.1016/j.geomorph.2016.10.030

Emre, Ö., Duman, T. Y., Doğan, A., Özalp, S., Tokay, F., & Kusçu, I. (2003). Surface faulting associated with the Sultandagı earthquake (Mw 6.5) of 3 February 2002, southwestern Turkey. *Seismological Research Letters*, *74*(4), 382–392. https://doi.org/10.1785/gssrl.74.4.382

Faccenna, C., & Becker, T. W. (2020). Topographic expressions of mantle dynamics in the Mediterranean. *Earth-Science Reviews*, *209*, 103327. https://doi.org/10.1016/j.earscirev.2020.103327

Faccenna, C., Becker, T. W., Auer, L., Billi, A., Boschi, L., Brun, J. P., et al. (2014). Mantle dynamics in the Mediterranean. *Reviews of Geophysics*, *52*(3), 283–332. https://doi.org/10.1002/2013RG000444

Faccenna, C., Becker, T. W., Jolivet, L., & Keskin, M. (2013). Mantle convection in the Middle East: Reconciling Afar upwelling, Arabia indentation and Aegean trench rollback. *Earth and Planetary Science Letters*, *375*, 254–269. https://doi.org/10.1016/j.epsl.2013.05.043

Faccenna, C., Bellier, O., Martinod, J., Piromallo, C., & Regard, V. (2006). Slab detachment beneath eastern Anatolia: A possible cause for the formation of the North Anatolian Fault. *Earth and Planetary Science Letters*, *242*(1–2), 85–97. https://doi.org/10.1016/j.epsl.2005.11.046

Fernández-Blanco, D., Bertotti, G., Aksu, A., & Hall, J. (2019). Monoclinal flexure of an orogenic plateau margin during subduction, south Turkey. *Basin Research*, *31*(4), 709–727. https://doi.org/10.1111/bre.12341

Fernández-Blanco, D., Mannu, U., Bertotti, G., & Willett, S. D. (2020). Forearc high uplift by lower crustal flow during growth of the Cyprus-Anatolian margin. *Earth and Planetary Science Letters*, *544*, 116314. https://doi.org/10.1016/j.epsl.2020.116314

Flecker, R., Ellam, R. M., Müller, C., Poisson, A., Robertson, A. H. F., & Turner, J. (1998). Application of Sr isotope stratigraphy and sedimentary analysis to the origin and evolution of the Neogene basins in the Isparta Angle, southern Turkey. *Tectonophysics*, *298*(1–3), 83–101. https://doi.org/10.1016/S0040-1951(98)00179-6

Flecker, R., Poisson, A., & Robertson, A. H. F. (2005). Facies and palaeogeographic evidence for the Miocene evolution of the Isparta Angle in its regional eastern Mediterranean context. *Sedimentary Geolology*, *173*(1–4), 277–314. https://doi.org/10.1016/j.sedgeo.2003.10.014

Flint, J. J. (1974). Stream gradient as a function of order, magnitude, and discharge. *Water Resources Research*, *10*(5), 969–973. https://doi.org/10.1029/wr010i005p00969

Forte, A. M., & Whipple, K. X. (2019). Short communication: The Topographic Analysis Kit (TAK) for TopoToolbox. *Earth Surface Dynamics*, *7*(1), 87–95. https://doi.org/10.5194/esurf7-87-2019

Gailleton, B., Mudd, S. M., Clubb, F. J., Peifer, D., & Hurst, M. D. (2019). A segmentation approach for reproducible extraction and quantification of knickpoints from river long profiles. *Earth Surface Dynamics*, *7*(1), 211–230. https://doi.org/10.5194/esurf-7-211-2019

Gallen, S. F. (2018). Lithologic controls on landscape dynamics and aquatic species evolution in postorogenic mountains. *Earth and Planetary Science Letters*, *493*, 150–160. https://doi.org/10.1016/j.epsl.2018.04.029

Gallen, S. F., & Wegmann, K. W. (2017). River profile response to normal fault growth and linkage: An example from the Hellenic forearc of south-central Crete, Greece. *Earth Surface Dynamics*, *5*(1), 161–186. https://doi.org/10.5194/esurf-5-161-2017

Glover, C. P., & Robertson, A. H. F. (1998a). Neotectonic intersection of the Aegean and Cyprus tectonic arcs: Extensional and strike-slip faulting in the Isparta Angle, SW Turkey. *Tectonophysics*, *298*(1–3), 103–132. https://doi.org/10.1016/S0040-1951(98)00180-2

Glover, C. P., & Robertson, A. H. F. (1998b). Role of regional extension and uplift in the Plio-Pleistocene evolution of the Aksu Basin, SW Turkey. *Journal of the Geological Society*, *155*(2), 365–387. https://doi.org/10.1144/gsjgs.155.2.0365

Güvercin, S. E., Konca, A. Ö., Özbakır, A. D., Ergintav, S., & Karabulut, H. (2021). New focal mechanisms reveal fragmentation and active subduction of the Antalya slab in the Eastern Mediterranean. *Tectonophysics*, *805*, 228792. https://doi.org/10.1016/j.tecto.2021.228792

Hack, J. T. (1957). Studies of longitudinal stream profiles in Virginia and Maryland. *Professional Paper*, (Vol. 294B). https://doi.org/10.3133/pp294b

Hack, J. T. (1973). Stream-profile analysis and stream-gradient index. *Journal of Research of the U. S. Geological Survey*, *1*, 421–429.

Haviv, I., Enzel, Y., Whipple, K. X., Zilberman, E., Matmon, A., Stone, J., & Fifield, K. L. (2010). Evolution of vertical knickpoints (waterfalls) with resistant caprock: Insights from numerical modeling. *Journal of Geophysical Research*, *115*(F3), F03028. https://doi.org/10.1029/2008JF001187

Howard, A. D., Seidl, M. A., & Dietrich, W. E. (1994). Modeling fluvial erosion on regional to continental scales. *Journal of Geophysical Research*, *99*(B7), 13971–13986. https://doi.org/10.1029/94JB00744

Howell, A., Jackson, J., Copley, A., McKenzie, D., & Nissen, E. (2017). Subduction and vertical coastal motions in the eastern Mediterranean. *Geophysical Journal International*, *211*(1), 593–620. https://doi.org/10.1093/gji/ggx307

Husson, L. (2006). Dynamic topography above retreating subduction zones. *Geology*, *34*(9), 741–744. https://doi.org/10.1130/G22436.1

Jaiswara, N. K., Pandey, P., & Pandey, A. K. (2019). Mio-Pliocene piracy, relict landscape and drainage reorganization in the Namcha Barwa syntaxis zone of eastern Himalaya. *Scientific Reports*, *9*(1), 1–11. https://doi.org/10.1038/s41598-019-54052-x

Jiang, W., Han, Z., Zhang, J., & Jiao, Q. (2016). Stream profile analysis, tectonic geomorphology and neotectonic activity of the Damxung-Yangbajain rift in the south Tibetan Plateau. *Earth Surface Processes and Landforms*, *41*(10), 1312–1326. https://doi.org/10.1002/esp.3899

Kanbur, S., & Öğretmen, N. (2022). Revised late Cenozoic foraminifer biostratigraphy of the Eskiköy Formation (Aksu Basin), SW Turkey and its paleoenvironmental conditions. *Palaeogeography, Palaeoclimatology, Palaeoecology*, *591*, 110883. https://doi.org/10.1016/j.palaeo.2022.110883

Karabıyıkoğlu, M., Çiner, A., Monod, O., Deynoux, M., Tuzcu, S., & Orcen, S. (2000). Tectonosedimentary evolution of the Miocene Manavgat Basin, Western Taurids, Turkey. In E. Bozkurt, J. A. Winchester, & J. D. A. Piper (Eds.), *Tectonics and magmatism in Turkey and the surrounding area* (Vol. 173, pp. 475–498). Geological Society.

Keller, E. A., & Pinter, N. (2002). *Active tectonics, earthquakes, uplift and landscape* (2nd ed., p. 362). Prentice Hall.

Kelletat, D., & Kayan, İ. (1983). Alanya batısındaki kıyılarda ilk C14 tarihlendirmelerinin ışığında Geç Holosen tektonik hareketleri. *TJK Bülteni*, *26*, 83–87.

Kelling, G., Robertson, A. H. F., & Buchem, F. V. (2005). Cenozoic sedimentary basins of southern Turkey: An introduction. *Sedimentary Geology*, *173*, 1–13.

Kirby, E., & Whipple, K. (2001). Quantifying differential rock-uplift rates via stream profile analysis. *Geology*, *29*(5), 415–418. https://doi.org/10.1130/0091-7613(2001)0292.0.CO;2

Kirby, E., & Whipple, K. X. (2012). Expression of active tectonics in erosional landscapes. *Journal of Structural Geology*, *44*, 54–75. https://doi.org/10.1016/j.jsg.2012.07.009

Kirby, E., Whipple, K. X., Burchfiel, B. C., Tang, W., Berger, G., Sun, Z., & Chen, Z. (2000). Neotectonics of the Min Shan, China: Implications for mechanisms driving Quaternary deformation along the eastern margin of the Tibetan plateau. *Geological Society of America Bulletin*, *112*(3), 375–393. https://doi.org/10.1130/0016-7606(2000)112%3C375:NOTMSC%3E2.0.CO;2

Kirby, E., Whipple, K. X., Tang, W., & Chen, Z. (2003). Distribution of active rock uplift along the eastern margin of the Tibetan plateau: Inferences from bedrock channel longitudinal profiles. *Journal of Geophysical Research*, *108*(B4), 2217. https://doi.org/10.1029/2001jb000861

Koçyigit, A., & Özacar, A. A. (2003). Extensional neotectonic regime through the NE edge of outer Isparta Angle, SW Turkey: New field and seismic data. *Turkish Journal of Earth Sciences*, *12*, 67–90.

Kounoudis, R., Bastow, I. D., Ogden, C. S., Goes, S., Jenkins, J., Braham, C. B., & Grant, C. (2020). Seismic tomographic imaging of the Eastern Mediterranean mantle: Implications for terminal stage subduction, the uplift of Anatolia, and the development of the North Anatolian Fault. *Geochemistry, Geophysics, Geosystems*, *21*(7), 2020GC009009. https://doi.org/10.1029/2020gc009009

Lague, D. (2014). The stream power river incision model: Evidence, theory and beyond. *Earth Surface Processes and Landforms*, *39*(1), 38–61. https://doi.org/10.1002/esp.3462

Larue, J. P. (2008). Effects of tectonics and lithology on long profiles of 16 rivers of the southern Central Massif border between the Aude and the Orb (France). *Geomorphology*, *93*(3–4), 343–367. https://doi.org/10.1016/j.geomorph.2007.03.003

Larue, J. P. (2011). Longitudinal profiles and knickzones: The example of the rivers of the Cher Basin in the northern French Massif Central. *Proceedings of the Geologists' Association*, *122*(1), 125–142. https://doi.org/10.1016/j.pgeola.2010.08.006

Liberatore, M., Gliozzi, E., Cipollari, P., Öğretmen, N., Spada, G., & Cosentino, D. (2022). Vertical velocity fields along the Eastern Mediterranean coast as revealed by late Holocene sea-level markers. *Earth-Science Reviews*, *234*, 104199. https://doi.org/10.1016/j.earscirev.2022.104199

Lv, L., Wang, L., Li, C., Li, H., Wang, X., & Wang, S. (2020). Formation mechanism for upland low-relief surface landscapes in the Three Gorges Region, China. *Remote Sensing*, *12*(23), 3899. https://doi.org/10.3390/rs12233899

Masek, J. G., Isacks, B. L., Gubbels, T. L., & Fielding, E. (1994). Erosion and tectonics at the margins of continental plateaus. *Journal of Geophysical Research*, *99*(B7), 13941–13956. https://doi.org/10.1029/94JB00461

McPhee, P. J., Altıner, D., & van Hinsbergen, D. J. J. (2018). First balanced cross section across the Taurides fold-thrust belt: Geological constraints on the subduction history of the Antalya slab in southern Anatolia. *Tectonics*, *37*(10), 3738–3759. https://doi.org/10.1029/2017TC004893

McPhee, P. J., Koç, A., & van Hinsbergen, D. J. J. (2022). Preparing the ground for plateau growth: Late Neogene Central Anatolian uplift in the context of orogenic and geodynamic evolution since the Cretaceous. *Tectonophysics*, *822*, 229131. https://doi.org/10.1016/j.tecto.2021.229131

Meijers, M. J. M., Brocard, G. Y., Cosca, M. A., Ludecke, T., Teyssier, C., Whitney, D. L., & Mulch, A. (2018). Rapid late Miocene surface uplift of the Central Anatolian Plateau margin. *Earth and Planetary Science Letters*, *497*, 29–41. https://doi.org/10.1016/j.epsl.2018.05.040

Monod, O., Kuzucuoğlu, C., & Okay, A. I. (2006). A Miocene Palaeovalley Network in the Western Taurus (Turkey). *Turkish Journal of Earth Sciences*, *15*(1), 1–23.

NASA Shuttle Radar. (2013). Topography Mission Global 1 arc second (SRTM). [Dataset]. https://doi.org/10.5067/MEaSUREs/SRTM/SRTMGL1.003

Öğretmen, N., Cipollari, P., Frezza, V., Faranda, C., Karanika, K., Gliozzi, E., et al. (2018). Evidence for 1.5 km of uplift of the Central Anatolian Plateau's southern margin in the last 450 kyr and implications for its multiphased uplift history. *Tectonics*, *37*(1), 359–390. https://doi.org/10.1002/2017TC004805

Okay, A. I., Zattin, M., & Cavazza, W. (2010). Apatite fission-track data for the Miocene Arabia-Eurasia collision. *Geology*, *38*(1), 35–38. https://doi.org/10.1130/g30234.1

Özgül, N. (1976). Toroslar'ın bazı temel jeolojik özellikleri. *Turkiye Jeoloji Kurumu Bulteni*, *19*, 5–78.

Pavano, F., Pazzaglia, F. J., & Catalano, S. (2016). Knickpoints as geomorphic markers of active tectonics: A case study from northeastern Sicily (southern Italy). *Lithosphere*, *8*(6), 633–648. https://doi.org/10.1130/L577.1

Perron, J. T., & Royden, L. (2013). An integral approach to bedrock river profile analysis. *Earth Surface Processes and Landforms*, *38*(6), 570–576. https://doi.org/10.1002/esp.3302

Pingel, H., Alonso, R. N., Altenberger, U., Cottle, J., & Strecker, M. R. (2019). Miocene to Quaternary basin evolution at the southeastern Andean plateau (Puna) margin (~24°S lat, Northwestern Argentina). *Basin Research*, *31*(4), 808–826. https://doi.org/10.1111/bre.12346

Poisson, A., Orszag-Sperber, F., Kosun, E., Bassetti, M. A., Muller, C., Wernli, R., & Rouchy, J. M. (2011). The late Cenozoic evolution of the Aksu basin (Isparta Angle; SW Turkey). New insights. *Bulletin de la Societe Geologique de France*, *182*(2), 133–148. https://doi.org/10.2113/gssgfbull.182.2.133

Poisson, A., Yağmurlu, F., Bozcu, M., & Şentürk, M. (2003). New insights on the tectonic setting and evolution around the apex of the Isparta Angle (SW Turkey). *Geological Journal*, *38*(3–4), 257–282. https://doi.org/10.1002/gj.955

Portner, D. E., Delph, J. R., Biryol, C. B., Beck, S. L., Zandt, G., Özacar, A. A., et al. (2018). Subduction termination through progressive slab deformation across Eastern Mediterranean subduction zones from updated P-wave tomography beneath Anatolia. *Geosphere*, *14*(3), 907–925. https://doi.org/10.1130/GES01617.1

Prince, P. S., & Spotila, J. A. (2013). Evidence of transient topographic disequilibrium in a landward passive margin river system: Knickpoints and paleo-landscapes of the New River basin, southern Appalachians. *Earth Surface Processes and Landforms*, *38*(14), 1685–1699. https://doi.org/10.1002/esp.3406

Racano, S., Jara-Muñoz, J., Cosentino, D., & Melnick, D. (2020). Variable Quaternary uplift along the southern margin of the Central Anatolian Plateau inferred from modeling marine terrace sequences. *Tectonics*, *39*(12). https://doi.org/10.1029/2019TC005921

Racano, S., Schildgen, T. F., Cosentino, D., & Miller, S. R. (2021). Temporal and spatial variations in rock uplift from river-profile inversions at the Central Anatolian Plateau southern margin. *Journal of Geophysical Research: Earth Surface*, *126*(8), 1–23. https://doi.org/10.1029/2020JF006027

Radeff, G., Schildgen, T. F., Cosentino, D., Strecker, M. R., Cipollari, P., Darbaş, G., & Gürbüz, K. (2017). Sedimentary evidence for late Messinian uplift of the SE margin of the Central Anatolian Plateau: Adana Basin, southern Turkey. *Basin Research*, *29*, 488–514. https://doi.org/10.1111/bre.12159

Reilinger, R., McClusky, S., Vernant, P., Lawrence, S., Ergintav, S., Cakmak, R., et al. (2006). GPS constraints on continental deformation in the Africa-Arabia-Eurasia continental collision zone and implications for the dynamics of plate interactions. *Journal of Geophysical Research*, *111*(B5). https://doi.org/10.1029/2005JB004051

Robertson, A. H. F. (1998). Tectonic significance of the Eratosthenes Seamount: A continental fragment in the process of collision with a subduction zone in the Eastern Mediterranean (Ocean Drilling Program Leg 160). *Tectonophysics*, *298*(1–3), 63–82. https://doi.org/10.1016/S0040-1951(98)00178-4

Schattner, U. (2010). What triggered the early-to-mid Pleistocene tectonic transition across the entire eastern Mediterranean? *Earth and Planetary Science Letters*, *289*(3–4), 539–548. https://doi.org/10.1016/j.epsl.2009.11.048

Scherler, D., Bookhagen, B., & Strecker, M. R. (2014). Tectonic control on 10Be-derived erosion rates in the Garhwal Himalaya, India. *Journal of Geophysical Research: Earth Surface*, *119*(2), 83–105. https://doi.org/10.1002/2013JF002955

Schildgen, T. F., Cosentino, D., Bookhagen, B., Niedermann, S., Yildirim, C., Echtler, H., et al. (2012a). Multi-phased uplift of the southern margin of the Central Anatolian plateau, Turkey: A record of tectonic and upper mantle processes. *Earth and Planetary Science Letters*, *317–318*, 85–95. https://doi.org/10.1016/j.epsl.2011.12.003

Schildgen, T. F., Cosentino, D., Caruso, A., Buchwaldt, R., Yildirim, C., Bowring, S. A., et al. (2012b). Surface expression of eastern Mediterranean slab dynamics: Neogene topographic and structural evolution of the southwest margin of the Central Anatolian Plateau, Turkey. *Tectonics*, *31*(2). https://doi.org/10.1029/2011TC003021

Schildgen, T. F., Yildirim, C., Cosentino, D., & Strecker, M. R. (2014). Linking slab breakoff, Hellenic trench retreat, and uplift of the Central and Eastern Anatolian plateaus. *Earth-Science Reviews*, *128*, 147–168. https://doi.org/10.1016/j.earscirev.2013.11.006

Schmid, S. M., Fügenschuh, B., Kounov, A., Maţenco, L., Nievergelt, P., Oberhänsli, R., et al. (2020). Tectonic units of the Alpine collision zone between Eastern Alps and western Turkey. *Gondwana Research*, *78*, 308–374. https://doi.org/10.1016/j.gr.2019.07.005

Schwanghart, W., & Scherler, D. (2014). Short communication: TopoToolbox 2 - MATLAB-based software for topographic analysis and modeling in Earth surface sciences. *Earth Surface Dynamics*, *2*(1), 1–7. https://doi.org/10.5194/esurf-2-1-2014

Şenel, M. (2002). *1/500.000 ölçekli Türkiye jeoloji haritası, Konya paftası*. MTA.

Şengör, A. M. C., Görür, N., & Şaroğlu, F. (1985). Strike slip faulting and related basin formation in zones of tectonic escape: Turkey as a case study. In K. D. Biddle & N. Christie-Blick (Eds.), *Strike- slip deformation, basin formation and sedimentation* (Vol. 17, pp. 227–264). Society of Economic Paleontologists and Mineralogists Special Publication.

Şengör, A. M. C., & Yilmaz, Y. (1981). Tethyan evolution of Turkey: A plate tectonics approach. *Tectonophysics*, *75*(3–4), 181–241. https://doi.org/10.1016/0040-1951(81)90275-4

Serpelloni, E., Faccenna, C., Spada, G., Dong, D., & Williams, S. D. P. (2013). Vertical GPS ground motion rates in the Euro-Mediterranean region: New evidence of velocity gradients at different spatial scales along the Nubia-Eurasia plate boundary. *Journal of Geophysical Research: Solid Earth*, *118*(11), 6003–6024. https://doi.org/10.1002/2013JB010102

Snyder, N. P., Whipple, K. X., Tucker, G. E., & Merritts, D. J. (2000). Landscape response to tectonic forcing: Digital elevation model analysis of stream profiles in the Mendocino triple junction region, northern California. *Geological Society of America Bulletin*, *112*(8), 1250–1263. https://doi.org/10.1130/0016-7606(2000)112<1250:LRTTFD>2.0.CO;2

Stearns, R. G. (1967). Warping on the Western Highland Rim Peneplain in Tennessee by groundwater sapping. *Geological Society of America Bulletin*, *78*(9), 1111–1124. https://doi.org/10.1130/0016-7606(1967)78[1111:WOTWHR]2.0.CO;2

Strecker, M. R., Alonso, R., Bookhagen, B., Carrapa, B., Coutand, I., Hain, M. P., et al. (2009). Does the topographic distribution of the central Andean Puna Plateau result from climatic or geodynamic processes? *Geology*, *37*(7), 643–646. https://doi.org/10.1130/G25545A.1

Tucker, G. E., & Whipple, K. X. (2002). Topographic outcomes predicted by stream erosion models: Sensitivity analysis and intermodel comparison. *Journal of Geophysical Research*, *107*(B9), ETG1-1–ETG1-16. https://doi.org/10.1029/2001JB000162

Üner, S., Özsayin, E., Kutluay, A., & Dirik, K. (2015). Polyphase tectonic evolution of the Aksu Basin, Isparta Angle (Southern Turkey). *Geologica Carpathica*, *66*(2), 157–169. https://doi.org/10.1515/geoca-2015-0017

Vandervoort, D. S., Jordan, T. E., Zeitler, P. K., & Alonso, R. N. (1995). Chronology of internal drainage development and uplift, southern Puna plateau, Argentine central Andes. *Geology*, *23*(2), 145–148. https://doi.org/10.1130/0091-7613(1995)023%3C0145:COIDDA%3E2.3.CO;2

VanLaningham, S., Meigs, A., & Goldfinger, C. (2006). The effects of rock uplift and rock resistance on river morphology in a subduction zone forearc, Oregon, USA. *Earth Surface Processes and Landforms*, *31*(10), 1257–1279. https://doi.org/10.1002/esp.1326

Wang, J., Hu, Z., Pan, B., Li, M., Dong, Z., Li, X., et al. (2019). Spatial distribution pattern of channel steepness index as evidence for differential rock uplift along the eastern Altun Shan on the northern Tibetan Plateau. *Global and Planetary Change*, *181*, 102979. https://doi.org/10.1016/j.gloplacha.2019.102979

Wdowinski, S., Ben-Avraham, Z., Arvidsson, R., & Ekström, G. (2006). Seismotectonics of the Cyprian Arc. *Geophysical Journal International*, *164*(1), 176–181. https://doi.org/10.1111/j.1365-246X.2005.02737.x

Whipple, K. X. (2004). Bedrock rivers and the geomorphology of active orogens. *Annual Review of Earth and Planetary Sciences*, *32*(1), 151–185. https://doi.org/10.1146/annurev.earth.32.101802.120356

Whipple, K. X., DiBiase, R. A., Ouimet, W. B., & Forte, A. M. (2017). Preservation or piracy: Diagnosing low-relief, high-elevation surface formation mechanisms. *Geology*, *45*(1), 91–94. https://doi.org/10.1130/g38490.1

Whittaker, A. C., Attal, M., Cowie, P. A., Tucker, G. E., & Roberts, G. (2008). Decoding temporal and spatial patterns of fault uplift using transient river long profiles. *Geomorphology*, *100*(3–4), 506–526. https://doi.org/10.1016/j.geomorph.2008.01.018

Wobus, C., Whipple, K. X., Kirby, E., Snyder, N., Johnson, J., Spyropolou, K., et al. (2006). Tectonics from topography: Procedures, promise, and pitfalls. In S. D. Willett, N. Hovius, M. T. Brandon, & D. M. Fisher (Eds.), *Tectonics, climate, and landscape evolution*, *Geological Society of America Special Paper, Penrose Conference Series*, (Vol. 398, pp. 55–74). https://doi.org/10.1130/2006.2398(04)

Yıldırım, C., Sarıkaya, M. A., & Çiner, A. (2016). Late Pleistocene intraplate extension of the Central Anatolian Plateau, Turkey: Inferences from cosmogenic exposure dating of alluvial fan, landslide, and moraine surfaces along the Ecemiş Fault Zone. *Tectonics*, *35*(6), 1446–1464. https://doi.org/10.1002/2015TC004038

Yıldırım, C., Schildgen, T. F., Echtler, H., Melnick, D., Bookhagen, B., Çiner, A., et al. (2013). Tectonic implications of fluvial incision and pediment deformation at the northern margin of the Central Anatolian Plateau based on multiple cosmogenic nuclides. *Tectonics*, *32*(5), 1107–1120. https://doi.org/10.1002/tect.20066

Yıldırım, C., Schildgen, T. F., Echtler, H., Melnick, D., & Strecker, M. R. (2011). Late Neogene and active orogenic uplift in the Central Pontides associated with the North Anatolian Fault: Implications for the northern margin of the Central Anatolian Plateau, Turkey. *Tectonics*, *30*(5). https://doi.org/10.1029/2010TC002756

Yıldırım, C., & Tüysüz, O. (2017). Estimation of the long-term slip, surface uplift and block rotation along the northern strand of the North Anatolian Fault Zone: Inferences from geomorphology of the Almacık Block. *Geomorphology*, *297*, 55–68. https://doi.org/10.1016/j.geomorph.2017.08.038